Materialia 7 (2019) 100382

Contents lists available at ScienceDirect

Materialia

journal homepage: www.elsevier.com/locate/mtla

Full Length Article

Modelling martensitic transformation in titanium alloys: The influence of temperature and deformation

Madeleine Bignon[a,b], Emmanuel Bertrand[a], Franck Tancret[a], Pedro E.J. Rivera-Díaz-del-Castillo[b,*]

[a] Institut des Matériaux Jean Rouxel (IMN), Université de Nantes, CNRS, Polytech Nantes, Rue Christian Pauc, Cedex 3, Nantes 44306, France
[b] Department of Engineering, Lancaster University, Lancaster LA1 4YK, UK

ARTICLE INFO

Keywords:
Titanium alloys
Martensite
TRIP
Superelasticity

ABSTRACT

New theory is presented to describe the occurrence of plasticity-induced transitions in titanium alloys. The approach is able to predict the composition dependence of transformation induced plasticity (TRIP), superelasticity, as well as martensite formation upon quenching. Martensite formation in the absence of stress is considered as the result of a competition between elastic strain energy and chemical driving force. Assuming that the formation of martensite is the result of a thermally activated nucleation process followed by athermal growth, a nucleation parameter is postulated to describe the conditions under which martensite is formed upon quenching; the parameter accounts for the ratio between the available thermal energy and an energy barrier for nucleation, suggesting that ω phase is not the main factor controlling martensite inhibition. This nucleation parameter is able to describe, for the first time, martensite occurrence in 130 alloys from the literature, quantifying the martensite start temperature (M_s) reported for 49 alloys with great precision. An empirical parameter ($[Fe]_{eq}$) is proposed and, when combined with the M_s prediction, it allows to define regions within which TRIP and superelasticity occur. By defining threshold values for the M_s, the $[Fe]_{eq}$ and the nucleation parameter, candidate alloys likely to display TRIP, superelasticity or martensitic transformation upon quenching can be identified. As a result, this method can be adopted to design alloys with tailored plasticity behaviour.

1. Introduction

Titanium alloys are used for various industrial applications including aircraft, medical devices and marine structures [1]. Among them, metastable β alloys have received special attention due to their deformation behaviour, sometimes displayed as transformation induced plasticity (TRIP), twinning induced plasticity (TWIP), shape memory or superelasticity effects. Superelasticity, observed in a variety of systems including nickel alloys, ferrous alloys and titanium alloys [2,3], is the capacity of an alloy to return to its original shape upon unloading even after having been deformed to strains of up to 7% or 8%. This property is used, for example, in orthodontic wires [4]. Alloys presenting shape memory can recover their original shape upon heating after having been deformed. Shape memory alloys have been used for various applications such as civil structures [5], actuators in robotics [6] or biomedical implants [7]. TRIP alloys exhibit excellent ductility and good work hardening rate. Benefit can be taken from their relatively low initial yield stress combined with a high work hardening rate to manufacture parts of intricate shapes; they are easily formable and the finished parts can reach a high yield stress, while keeping significant ductility. Automotive industry has adopted TRIP steels for structural parts such as bumpers, and although several studies on TRIP titanium alloys insist on their suitability for biomedical implants [8], their properties make them interesting candidates for structural applications as well.

The deformation behaviour of β titanium alloys is strongly composition dependent and is generally assumed to be controlled by the stability of the high temperature body-centred cubic (BCC) β phase [9]. This stability can be increased by β stabilisers such as Fe, Mo, V or Cr and it can be decreased by elements stabilising the low temperature hexagonal close-packed (HCP) phase such as Al or O. A minimum quantity of β stabilisers is necessary to retain the BCC phase at room temperature and it is reported that the least stable β alloys exhibit stress-induced martensite transformation, leading to TRIP effect when the martensite is mechanically stable or superelasticity when it is unstable. Upon increasing the concentration in β stabilisers, the deformation mode is believed to switch to twinning, and when their concentration is further increased, the deformation only occurs by dislocation glide [9] in a single stable β

* Corresponding author.
E-mail address: p.rivera1@lancaster.ac.uk (P.E.J. Rivera-Díaz-del-Castillo).

https://doi.org/10.1016/j.mtla.2019.100382
Received 12 June 2019; Accepted 18 June 2019
Available online 6 July 2019

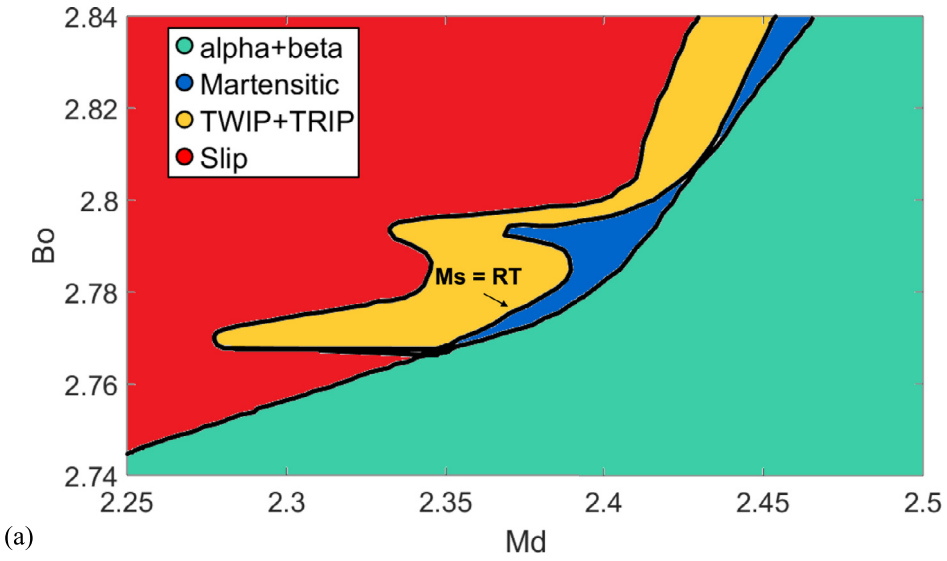

(a)

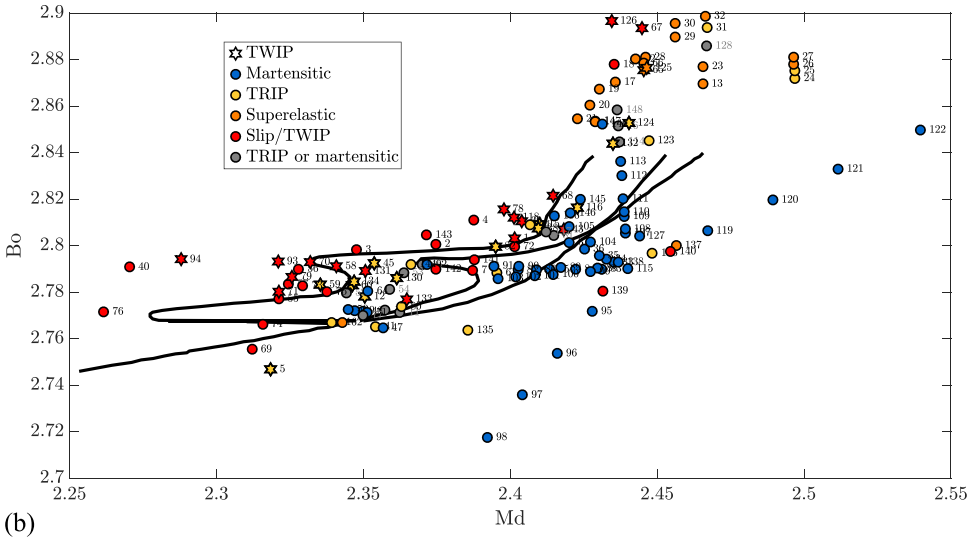

(b)

Fig. 1. (a) Reproduction of the Bo–Md map from [10]. The four coloured zones correspond to the four expected types of behaviour according to Morinaga's method. (b) Alloys from the literature disposed on the map from Morinaga. The experimentally observed behaviour of the alloys is indicated by the colour of the bullets (or by their number, with number code as shown in Appendix A.) (For interpretation of the references to colour in this figure legend, the reader is referred to the web version of this article.).

phase. However, the mechanisms involved in the stress-induced transformations are not fully understood yet.

A number of criteria have been adopted to design TRIP and TWIP titanium alloys. A useful tool to predict β phase retention is the empirical Mo equivalent ($[Mo]_{eq}$) parameter [9]. The criterion based on this parameter is reliable but discards a certain number of β alloys that have been shown to display TRIP. The most famous design tool for TRIP and TWIP alloys is the method initially proposed by Morinaga et al. [10], sometimes called "Bond Order method". It consists in mapping alloys as a function of two composition-dependent electronic parameters: the bond order between atoms (Bo) and the metal d-orbital level (Md). The position of the Ti-alloys on the map allows to identify their deformation behaviour. The original map in [10] is reproduced in Fig. 1a. Although this approach has proven its effectiveness in designing numerous new TRIP/TWIP compositions [11–13], it displays some limitations. The so-called phase stability map has been determined from existing systems, but some TRIP or TWIP alloys lie outside the drawn borders (see Fig. 1b), so that it is likely that many others exist in unexplored composition ranges. One aim of this work is to propose a new approach to design alloys undergoing martensitic transformation upon deformation.

A model combining thermodynamics and micromechanics is proposed here to describe the martensite formation. It is assumed that the nucleation of martensite during quenching is a thermally activated process requiring an energy barrier to be overcome. An expression for this barrier is suggested, leading to the definition of a nucleation parameter that allows to predict whether martensitic transformation occurs upon quenching. Considering that martensite growth is the result of a competition between elastic strain energy and chemical driving force, a martensite stabilisation temperature (M_s^*), which corresponds to the experimental M_s when the energy barrier can be overcome, is calculated. Then, a criterion combining M_s^* and a new empirical parameter ($[Fe]_{eq}$) is proposed to identify the composition dependence of TRIP, superelasticity or slip/twinning. This is the first approach capable to predict the occurrence and composition dependence of such wide range of transformation and deformation behaviours.

2. Microstructure at room temperature

In order to design alloys displaying tailored deformation behaviour such as TRIP, TWIP, superelasticity or shape memory effect, it is first required to predict their microstructure at room temperature. Quenched titanium alloys can be roughly divided into two categories. Firstly, alloys that form martensite upon quenching, and which microstructure at room temperature (prior to deformation) is either fully martensitic or a mixture of martensite and β phase. The martensite can either have

an HCP structure, designated as α', or an orthorhombic crystal structure, designated as α'' [14]. The alloys of this category will hereon be referred to as martensitic. The second category consists of alloys that exhibit only β phase at room temperature. They will hereon be referred to as β alloys. It is generally thought that the latter have an M_s below room temperature, but no experimental evidence supports this hypothesis: some metastable β alloys have been quenched down to cryogenic temperatures and still display no martensite [15,16]. The purpose of this section is to propose a method to predict whether an alloy is martensitic after quenching, and to calculate M_s if it is martensitic. The range of factors influencing the transformation include the Gibbs free energy, the elastic energy, the presence of martensite nucleation sites, the grain size and the quench rate. These are accounted for in the theory presented in this and the forthcoming section.

2.1. Martensite start temperature calculation

2.1.1. Model

In order to estimate the M_s temperature, the change in energy ΔG associated with the martensite product, treated here as an ellipsoidal inclusion in the BCC β phase, is computed as described by Wollants et al. [17].

$$\Delta G = 2\pi r^2\gamma - \frac{4}{3}\pi r^2 c(\Delta g_{ch} - \Delta g_{el}) \tag{1}$$

where c is the semi thickness of the martensite ellipsoidal inclusion, r is its radius, Δg_{ch}[1] is the volumetric chemical driving force. $\Delta g_{ch} = g_\beta - g_{\alpha'}$ where g_β and $g_{\alpha'}$ are respectively the Gibbs free energies of the BCC and the HCP phases. This quantity is computed employing thermodynamic software (Thermo-Calc®) and 'TCTI1' thermodynamic titanium database[2], and by assuming that the free energy of the orthorhombic phase α'' can be approximated by the free energy of the HCP phase α' (discussed in Section 5.3). Δg_{el} is the volumetric elastic strain energy induced by the presence of the plate; γ is the interfacial energy per unit area of product phase. The interfacial and elastic energies oppose the transformation.

Computation of the elastic strain energy

The eigenvalues of the strain tensor describing the transformation from the BCC structure to the orthorhombic or HCP structure are [14]:

$$\lambda_1 = \frac{a_{\alpha^i} - a_\beta}{a_\beta} \tag{2}$$

$$\lambda_2 = \frac{b_{\alpha^i} - \sqrt{2}a_\beta}{\sqrt{2}a_\beta} \tag{3}$$

$$\lambda_3 = \frac{c_{\alpha^i} - \sqrt{2}a_\beta}{\sqrt{2}a_\beta} \tag{4}$$

where a_β is the lattice parameter of the BCC structure, a_{α^i}, b_{α^i} and c_{α^i} are the lattice parameters of the martensitic phase, where α^i designates α' if the martensite is HCP and α'' if it is orthorhombic. The expression for the lattice parameters as a function of composition can be found in the literature for binary alloys, and the elemental contributions are assumed to be additive. The expressions employed for lattice parameters calculation are provided in Appendix B.

The elastic strain energy is computed by considering an ellipsoidal martensite plate in an infinite homogeneous isotropic elastic medium. The martensite is considered to be elastically isotropic. The strain tensor is divided into its deviatoric and hydrostatic components, as suggested by Olson and Cohen [19], so that the elastic strain energy Δg_{el} can be divided into a transformation volume-change term (Δg_{el}^{dil}) and a shape-change term (Δg_{el}^{shape}), with $\Delta g_{el} = \Delta g_{el}^{dil} + \Delta g_{el}^{shape}$.

The volume change is approximated by a pure dilatation and the associated elastic energy is computed as described by Eshelby [20]:

$$\Delta g_{el}^{dil}(T) = \frac{2}{9}\frac{(1+\nu)}{(1-\nu)} \cdot \mu(T) \cdot \left(\frac{\Delta V}{V}\right)^2 \tag{5}$$

where ν is the Poisson's ratio, taken here as equal to $\frac{1}{3}$, $\mu(T)$ is the shear modulus at temperature T, computed as described by Galindo-Nava [21]:

$$\mu(T) = \mu_{RT}(k_1 + k_2 T) \tag{6}$$

where μ_{RT} is the composition-dependent shear modulus at room temperature (RT), obtained by a mixture rule, T is the absolute temperature, k_1 and k_2 are the fitted constants described in [21] and yield $k_1 = 1 + \frac{19.63689}{2(1+\nu)}$ and $k_2 = -\frac{0.07193}{2(1+\nu)}$.

$\frac{\Delta V}{V}$ is the relative change in volume accompanying the transformation:

$$\frac{\Delta V}{V} = \left(\frac{1}{3}(\lambda_1 + \lambda_2 + \lambda_3) + 1\right)^3 - 1 \tag{7}$$

The shape change is approximated by a pure shear and is computed as described by Eshelby [20]:

$$\Delta g_{el}^{shape}(T) = \mu(T) \cdot \frac{\pi}{2}\frac{(2-\nu)}{(1-\nu)} \cdot \epsilon^2 \cdot \frac{c}{r} = K(T)\frac{c}{r} \tag{8}$$

$K(T)$ is introduced in Eq. (8) to shorten the notation, ϵ is the shear component of the strain associated with the phase transformation [19] and is composition dependent via the lattice parameters:

$$\epsilon = \sqrt{\frac{1}{6}\left((\epsilon_1 - \epsilon_2)^2 + (\epsilon_2 - \epsilon_3)^2 + (\epsilon_3 - \epsilon_1)^2\right)} \tag{9}$$

where ϵ_1, ϵ_2 and ϵ_3 are the eigenvalues of the deviatoric component of the strain tensor ($\epsilon_i = \lambda_i - \frac{1}{3}(\lambda_1 + \lambda_2 + \lambda_3)$)

Computation of M_s

By combining (1), (5) and (8):

$$\Delta G(T) = 2\pi r^2\gamma - \frac{4}{3}\pi c r^2\left(\Delta g_{ch}(T) - \Delta g_{el}^{dil}(T)\right) + \frac{4}{3}\pi c^2 r K(T) \tag{10}$$

Above T_0, nucleation cannot occur and the alloy only displays β phase (Fig. 2a). The nucleation of a product embryo of semi-thickness c_0 and radius r_0 occurs below the temperature at which the HCP and BCC Gibbs free energies are equal (T_0). Then, as explained by Wollants et al. [17], when the temperature is such that $\frac{\partial \Delta G}{\partial r} < 0$, the embryo grows radially (increase of r, Fig. 2b), until it is blocked by a strong obstacle (e.g. a grain boundary) and reaches a radius $a/2$, where a is the size of the parent grain (Fig. 2b). From that point, the particle continues to thicken in the direction normal to the plate plane (increase of the semi-thickness c), until it reaches a state such that the growth does not allow the system to further reduce its energy and a local equilibrium is reached at the interface between the parent and product

[1] The convention adopted here is such that the driving force is positive when the transformation is promoted

[2] Calculations were performed as well with the concurrent database 'TTTI3' which produced similar results. Another database specific to β titanium alloys labelled 'Ti-Gen' has been proposed by Yan and Olson [18]. To validate this database, these authors showed that they could obtain good agreement between experimental values of M_s, and values of M_s extracted from Ti-Gen database. However, the model they used to compute M_s included both values from the Ti-Gen database and fitting parameters. Therefore, potential inaccuracy in the database would be corrected by the fitting parameters, so that the adequacy of Ti-Gen can only be proven in the frame of this M_s model. As soon as other equations are used to compute M_s, we therefore have no guarantee of the accuracy of the database. Since the approach used here is different than Yan's approach, using Ti-Gen has not been attempted. In addition, elements present in either TTTI3 or Ti-Gen would allow their application to a much reduced number of alloys than TCTI1.

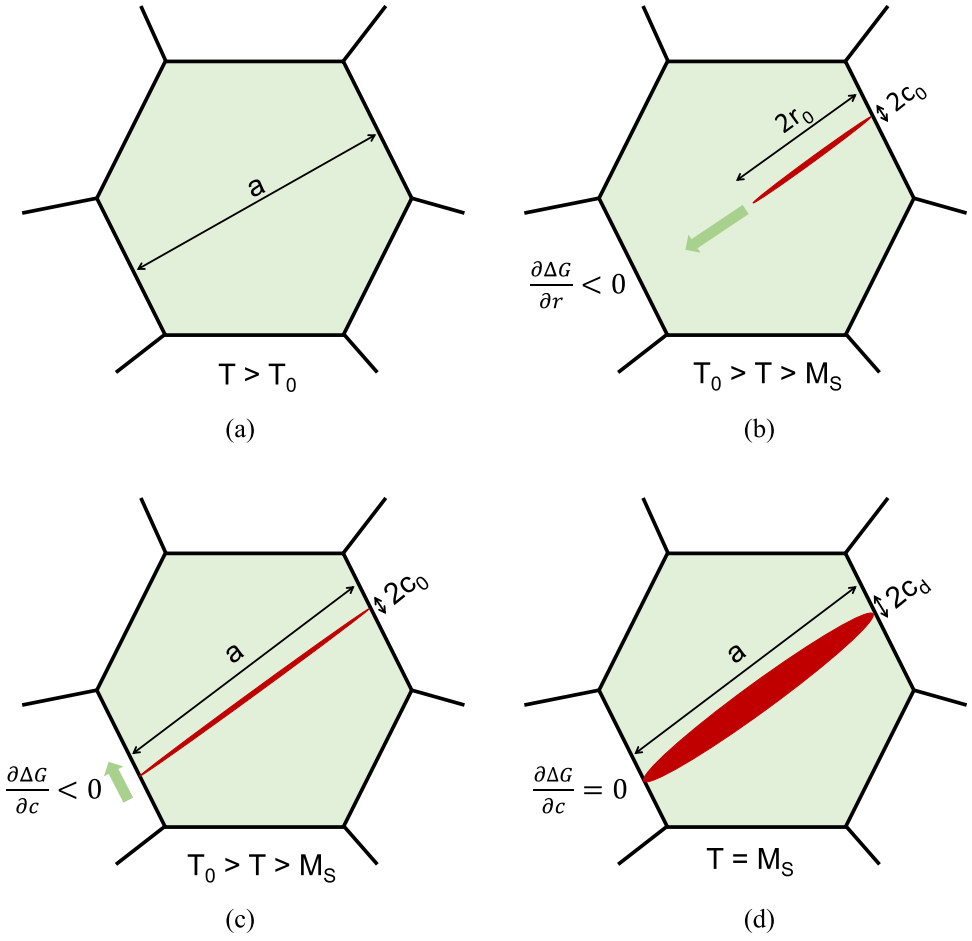

Fig. 2. Martensite nucleation and growth. (a) BCC β phase at a temperature above T_0 (b) A martensite embryo nucleates and starts growing radially (c) Radial growth is stopped by a grain boundary and the thickening starts. (d) A local thermoelastic equilibrium is reached and the thickening stops. Further cooling is necessary for the thickening to continue.

phases (Fig. 2d). The condition for such an equilibrium is: $\frac{\partial \Delta G}{\partial c} = 0$ [17]. When a product plate is formed from an existing defect, this condition is obtained by derivating Eq. (10):

$$\Delta g_{ch} - \Delta g_{el}^{dil} - 2K\frac{c}{r} = 0 \tag{11}$$

Let us label c_d the minimal detectable semi-thickness for a martensite plate. This detectable semi-thickness is set to 50 nm; this roughly matches the usual minimal thickness that is experimentally reported[3]. Then, if a is the grain size, we define the martensite stabilisation temperature M_s^* as the temperature at which a plate of martensite reaches a detectable size:

$$\Delta g_{ch}(M_s^*) - \Delta g_{el}^{dil}(M_s^*) - 2K(M_s^*)\frac{c_d}{a/2} = 0 \tag{12}$$

Any further cooling leads to further thickening, until the martensite finish temperature is reached (M_f) and the transformation is complete. The martensite stabilisation temperature M_s^* is defined as the highest temperature at which martensite can reasonably experimentally be observed if nucleation has happened, and should therefore be very close from the experimental martensite start temperature.

[3] For example, Gao et al. investigated the deformed microstructure of a TWIP/TRIP titanium alloy at different strain levels [12]; for the lowest strain at which martensite plates were observed, they were approximately 100 nm thick (50 nm semi-thickness). Very detailed microstructural investigation was also performed by Zhang et al. in a TRIP/TWIP alloy; they reported the presence of 30–150 nm thick martensite plates [22]. It therefore seems reasonable to assume that in the general case, the presence of a few plates of martensite less than 100 nm thick might go unnoticed, which justifies the chosen detectable limit.

M_s^* is obtained by iteratively computing the quantity on the left hand side of Eq. (12) for different temperatures. Since the elastic strain energy depends on the structure of the martensite (α'' or α'), M_s^* is calculated twice for each composition, by assuming both an HCP martensite and an orthorhombic martensite (see Appendix B). The retained M_s^* is the highest of both. A flow diagram for this calculation is shown in Fig. 3.

The martensite temperature calculated here is taken to be that at which a plate of martensite reaches a detectable size. The computation of M_s^* is thus based on a criterion regarding the growth of the martensite and not its nucleation. Indeed, the equations described above are valid for an existing martensite plate. M_s^* is computed by assuming that the nucleation has already taken place at a temperature somewhere in between M_s^* and T_0. This last point is developed in Section 2.2.

The method described above has been applied to calculate the M_s^* temperature of alloys from literature. Since the calculation depends on the grain size a, which is not always reported, an average value of 100 μm has been assumed for all alloys (the grain size dependency will be discussed in Section 5.3). Fig. 4 shows the calculated M_s^* for different alloys together with their type of behaviour during plastic deformation. Referring to Fig. 4, when the M_s^* is approximately below −100 °C, martensite is not reported, neither upon quenching nor the application of an external stress. The alloys for which the M_s^* is around or just below room temperature are mostly superelastic. For these alloys, when an external stress is applied, the driving force necessary for the martensitic transformation is supplied by the external work, but when the stress is removed, the martensite is no longer stable and reverses back to β phase. TRIP alloys entirely retain the β phase following quenching, but the M_s^* for most of them lies in the range 100–300°C. Nevertheless, the calculation of M_s^* is not inconsistent with their behaviour. Indeed, for

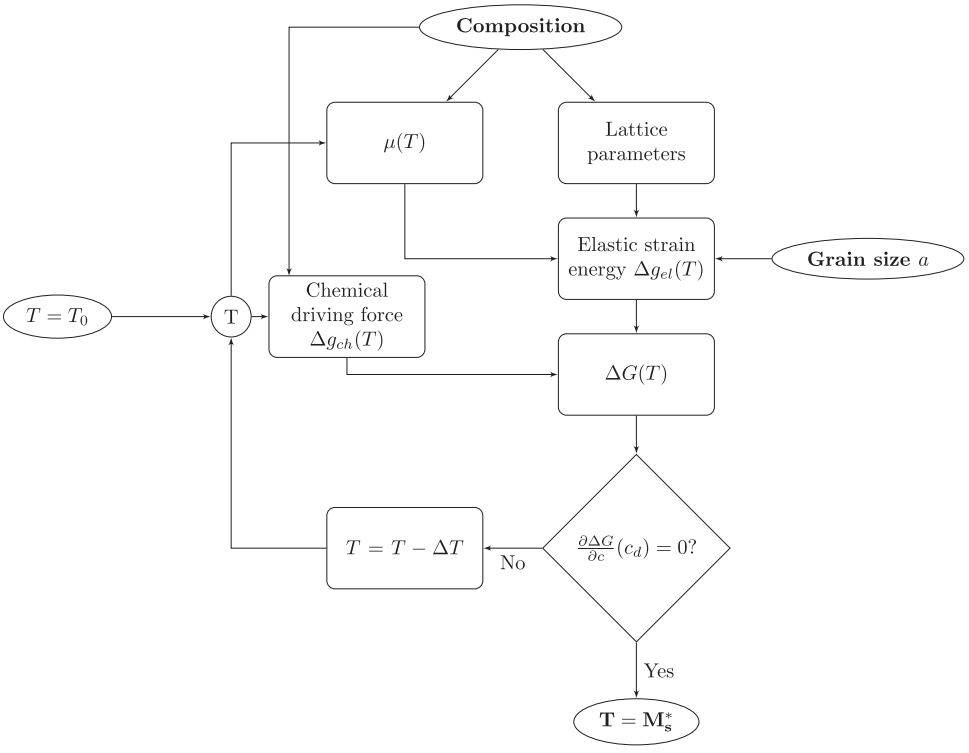

Fig. 3. Flow diagram for M_s^* calculation.

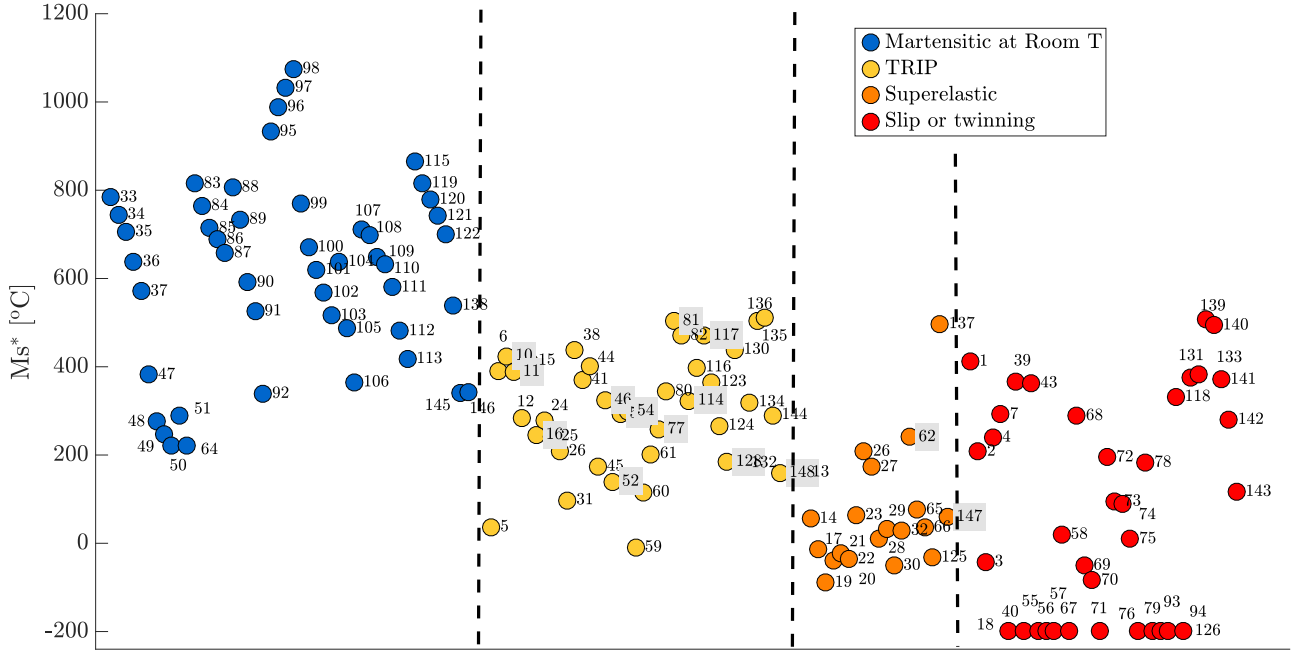

Fig. 4. Calculated M_s^* for alloys grouped as martensitic at room temperature, TRIP, superelastic or slip/twinning (from left to right, the dotted lines separate the different types of behaviour). The horizontal axis is only to spread the alloys in the panel. The alloys which number is written in a grey background display TRIP, but have also been seen martensitic under certain experimental conditions. When the calculations indicated that there was no temperature for which martensite is thermomecanically more stable than β, the M_s^* has been set to −200 °. The number code for each composition is shown in Appendix A.

TRIP alloys, when an external stress is applied, the martensitic transformation is induced and does not reverse when the load is released, which means that the martensite is probably stable at room temperature and that it cannot be assumed that M_s lies below room temperature. The model rightly predicts that martensite should be stable at room temperature.

In the case of TRIP alloys, it may seem paradoxical that the calculated M_s^* lies above room temperature when the experimental evidence shows that no martensite forms upon quenching. The reason for this is that the M_s^* computation implicitly considers that martensite nucleation has already taken place when the M_s^* is reached. It may therefore be assumed that in TRIP alloys, *nucleation* is inhibited upon

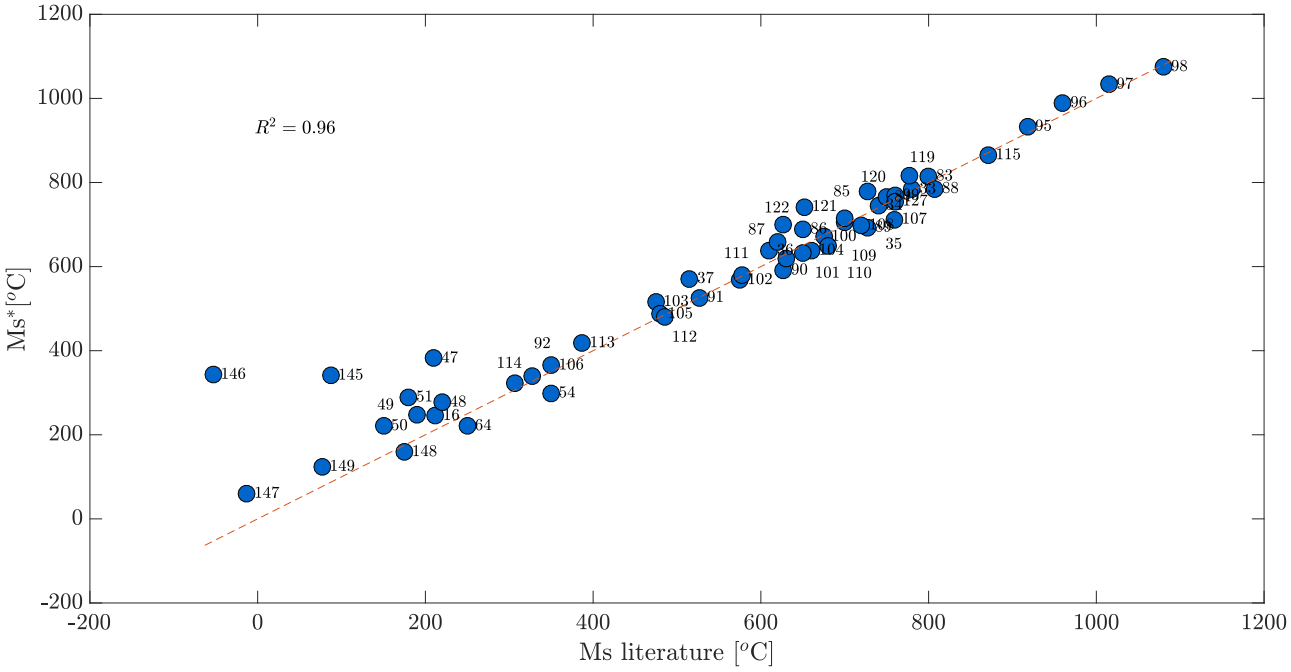

Fig. 5. Calculated M_s^* and experimental values for M_s obtained upon quenching. The number code for each composition is shown in Appendix A.

quenching, and that at room temperature the external work triggers nucleation. Once the martensite has nucleated due to external work, the growth can athermally start. As a consequence, it seems necessary to have a tool that allows to predict if the nucleation of martensite is likely to occur upon quenching, or if the nucleation requires external work.

Fig. 5 shows a comparison between the calculated M_s^* and the experimental M_s, when this experimental M_s is measured during cooling and the transformation occurs in the absence of external stress. Some martensitic alloys appear in Fig. 4 but not in Fig. 5, these compositions are known to be martensitic after quenching but no information was found regarding their M_s.

2.2. Martensite nucleation upon quenching

TRIP alloys display β microstructure after quenching, even though M_s^* computation indicates that martensite should be stable at room temperature (see Fig. 4). The competition between martensite and ω phase is a plausible hypothesis to explain the absence of martensite [18]. Although ω formation during cooling may play a role in martensite inhibition, thermodynamic calculations suggest that it is not necessary to invoke ω phase formation to explain the stabilisation of β phase at room temperature, as will be discussed in Section 5.2. The purpose of this section is to propose an explanation for the stabilisation of the β phase at room temperature, and a method to quantify it.

2.2.1. Model

Olson and Cohen [23] have shown that the first step of the transition from the BCC to HCP phase can be rationalised as the dissociation of a $\frac{1}{2}[111]$ screw dislocation on a $(1\bar{1}0)$ plane into three partials according to the reaction $\frac{1}{2}[111]=\frac{1}{8}[110]+\frac{1}{4}[112]+\frac{1}{8}[110]$ [24]. Assuming that the lattice opposes the glide of the dissociating partials, an energy barrier must be overcome for the dislocation to split into partials (corresponding to a high energy transition state between BCC and HCP, or to the energy necessary for the first steps of the dissociation of a perfect dislocation into partials). This energy barrier could, for example, be similar to a Peierls barrier (as it represents an opposition to the glide of a partial dislocation), and thus, if the energy barrier per dislocation is labeled E^*, it could have a form such as [25]:

$$E^*(T) = \chi b^3 \mu(T) \tag{13}$$

where χ is a constant independent from composition, b is the magnitude of the Burgers vector of the screw dislocation, calculated as $b = \frac{1}{2}\sqrt{3}a_\beta$. This energy barrier is assumed to be overcome by thermal fluctuations. For a characteristic dislocation vibration of frequency f_0, the energy barrier is successfully overcome at a rate f [25]:

$$f(T) = f_0 \cdot \exp(-E^*(T)/(kT)) \tag{14}$$

where k is the Boltzmann constant. The nucleation rate of martensite is expressed as:

$$\frac{dN}{dt} = N_0 \cdot f(T) = N_0 \cdot f_0 \cdot \exp(-E^*(T)/(kT)) \tag{15}$$

where N_0 is the number density of potential nucleation sites. If the cooling occurs at a cooling rate $Q = -\frac{dT}{dt}$, from Eq. (16) comes:

$$\frac{dN}{dT} = -\frac{N_0}{Q} \cdot f(T) = -\frac{N_0}{Q} \cdot f_0 \cdot \exp(-E^*(T)/(kT)) \tag{16}$$

By dividing the cooling process in elementary ΔT temperature steps, the number of embryos that nucleate at each step yields:

$$\Delta N(T) = \left|\frac{dN}{dT}\Delta T\right| = \frac{N_0 \cdot |\Delta T|}{Q} \cdot f(T) \tag{17}$$

The nucleation of martensite is assumed to start around T_0 as the maximum temperature at which a martensitic embryo can potentially form, and it is therefore the temperature at which the thermal energy for nucleation is maximum and the energy barrier is minimum (the barrier is proportional to the shear modulus which linearly decreases with temperature). Since there is no martensite nucleus above T_0, the number density $N(T_0)$ of martensite embryos nucleating during the first step of the transformation can be approximated by $\left(\frac{dN}{dT}\right)_{T_0} \cdot \Delta T$. Thus, according to Eqs. (14) and (17):

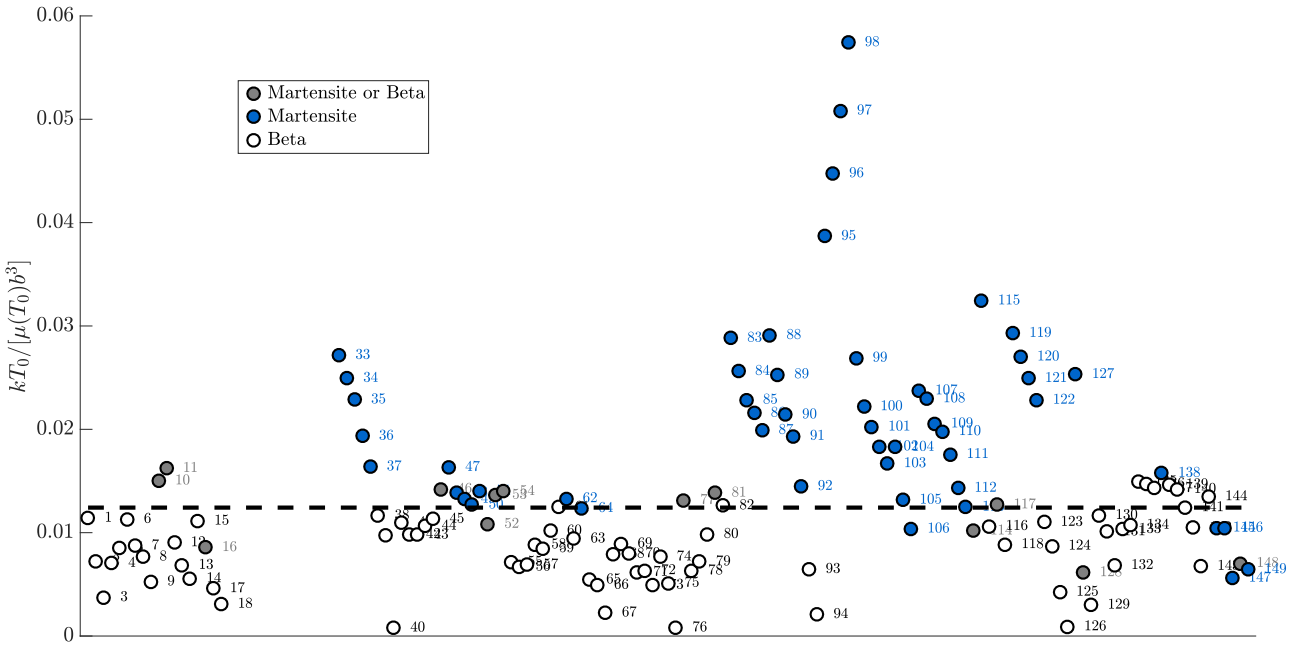

Fig. 6. Nucleation parameter, calculated for alloys from the literature. The horizontal line is the threshold that is found to separate the martensitic alloys from the β alloys. The horizontal axis is only to spread the alloys in the chart. The alloys referred to as "martensitic or β" are the ones that have been reported martensitic or β depending on the experimental conditions. The number code for each composition is shown in Appendix A.

$$N(T_0) = \frac{Q_0}{Q} \cdot N_0 \cdot \exp(-E^*(T_0)/(kT_0)) \tag{18}$$

where $Q_0 = |\Delta T| \cdot f_0$

The number of martensite nuclei appearing at any lower temperature interval is assumed to scale with the number density of nuclei at T_0, so that the total number of nuclei should be roughly proportional to $N(T_0)$. Therefore, there should exist a critical number density of martensite nuclei N_m, such that nucleation can be considered as occurring only if $N(T_0) > N_m$. From Eqs. (13) and (18), the condition for the martensite nucleation upon quenching is:

$$\frac{kT_0}{\mu(T_0)b^3} > \frac{\chi}{\ln(\frac{N_0}{N_m}\frac{Q_0}{Q})} \tag{19}$$

On the left hand side of Inequation (19), the term kT_0 is the available thermal energy for nucleation at the first stages of transformation and the term $\mu(T_0)b^3$ is proportional to the energy barrier for nucleation. The term $\frac{kT_0}{\mu(T_0)b^3}$ therefore scales with the ratio between an available thermal energy and a required energy for nucleation; it will hereon be referred to as "nucleation parameter". The nucleation parameter strongly depends on composition, through the partitionless equilibrium temperature T_0 between β and α', coming from Thermo-Calc®, and through the shear modulus. Inequation (19) indicates that martensite can nucleate during cooling only if the nucleation parameter exceeds a certain value, which will be referred to hereon as "critical nucleation parameter". This critical nucleation parameter depends on the cooling rate but is composition independent. By separating the alloys from the literature into two groups (martensitic and β), and computing for each of them the value of the nucleation parameter, the value of the critical nucleation parameter can thus easily be fitted.

2.2.2. Application to alloys from literature

The nucleation parameter is computed for different alloys from the literature as shown in Fig. 6, where it is clear that a critical nucleation parameter set as $[\ln(\frac{N_0}{N_m}\frac{Q_0}{Q})]^{-1} \cdot \chi = 1.24 \cdot 10^{-2}$ allows to separate martensitic from β alloys. This value is assumed to be valid for a conventional cooling rate. The nucleation parameter is also calculated for binary systems, and shown in Fig. 7. The black dotted line shows the limit to retain β at room temperature. In order to compare this with the available experimental data, the critical compositions necessary to retain β at room temperature are extracted from the literature and gathered in Table 1. The threshold of $1.24 \cdot 10^{-2}$ is also used to calculate, for each binary system, the critical composition necessary to retain β at room temperature. These calculated values are plotted as a function of experimental data from Table 1 in Fig. 8.

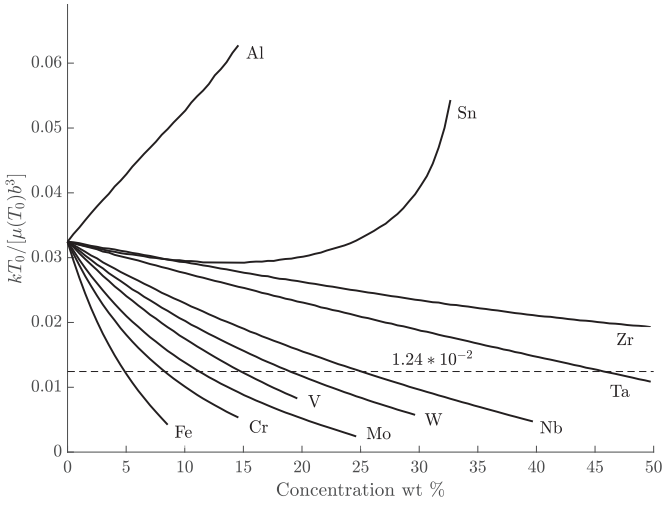

Fig. 7. Calculation of the nucleation parameter for binary systems. The dotted line shows the threshold expected to delimitate the martensitic alloys from the β alloys after quenching.

3. Identifying TRIP, superelastic and slip/TWIP alloys

This section proposes parameters to identify TRIP, superelasticity, and alloys deforming by dislocation slip or twinning. In this work, TRIP effect is defined as the formation of martensite upon deformation with-

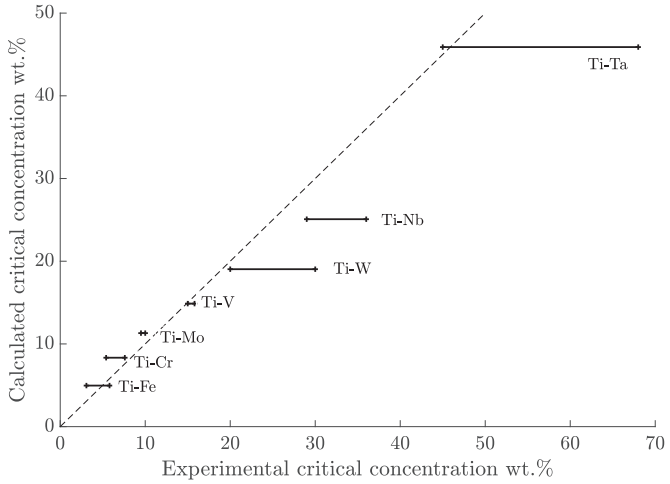

Fig. 8. Calculation of the critical concentration to retain β upon quenching for different binary systems as a function of the experimental data. The horizontal lines represent the experimental ranges of critical compositions found in the literature, which references are shown in Table 1. The dotted line is shown for reference.

Table 1
Critical compositions necessary to retain β phase upon quenching in binary alloys, extracted from the literature.

Element	Minimum concentration necessary to retain β upon quenching in wt %
Fe	3.5 [26], 5.8 [27], between 3.08 and 4.07 [28]
Cr	6.5 [26], 7.6 [27], between 5.4 and 6.5 [28]
Mo	10 [26], 9.5 [27]
V	15 [26], 15.8[27], about 15 [28]
W	22.5[26], 30 [27], between 20 and 25 [28]
Nb	29 [29](high quenching rate) 36 [27]
Ta	45 [26], 68 [27]

out reversion to β upon unloading, whereas the alloys referred to as superelastic are the ones in which the martensite that forms upon deformation reverses upon unloading. So far, no solution was found to predict twinning occurrence, so the alloys referred to as "TRIP" may also display twinning, as often observed experimentally. Alloys referred to as "slip or twinning" may or may not display TWIP but do not display martensitic transformation.

Identifying slip and TWIP alloys

In the present section, we focus on alloys that are fully β at room temperature. As the concentration in β stabilisers increases, the deformation behaviour generally switches from stress-induced martensite (TRIP or superelasticity), to TWIP or dislocation slip. This transition cannot be explained solely by the value of M_s^* (Fig. 4). It is assumed that, for such alloys the critical stress for triggering the nucleation of martensite is too great and that twinning or dislocation glide is energetically more favourable. The critical stress to trigger martensite, dislocation glide or twinning could not be assessed in the present work. An empirical criterion is instead proposed; inspired but differing from the $[Mo]_{eq}$. The $[Mo]_{eq}$ had been built thanks to experimental data on binary alloys in order to predict the tendency of an alloy to retain the β phase *upon quenching*. The proposed Fe equivalent ($[Fe]_{eq}$) criterion is tailored to experimental data in order to describe the tendency to retain β *upon deformation*.

The suggested criterion uses Fe as a reference element because it has the strongest stabilizing effect on the β phase. The proposed "$[Fe]_{eq}$" criterion is obtained in the following way: the coefficient to each term in Eq. (20) is obtained by dividing the critical concentration of Fe necessary to retain β under deformation in the Ti–Fe system by the critical concentration necessary to retain β under deformation in the given binary system. When this critical composition was not found in the literature, it has been extrapolated from multicomponent alloys. In the case of Cr and Fe binary systems, no composition has been reported to display TRIP; therefore, it is assumed that, for these strong β stabilisers, the critical concentration to retain β upon deformation is very close to, or lower than the critical composition to retain β at RT. The critical compositions considered for the $[Fe]_{eq}$ expression are gathered in Table 2, together with the compositions that were used to determine their values. Since in the case of the Ti–Fe system, the critical concentration necessary to retain β upon deformation has been evaluated to [Fe]= 3.5 wt% (Table 2), the compositions such that the $[Fe]_{eq}$ exceeds 3.5% are expected to inhibit the martensitic transformation under deformation. The assessment of this criterion on multicomponent alloys will be presented later.

Table 2
Critical compositions necessary to retain the β phase upon deformation in binary alloys, calculated and extrapolated from data available in the literature.

Element	Adopted limit wt.% composition for SIM	Alloys used as references
Fe	3.5	Ti–10Mo, Ti–10Mo–1Fe [30]
Cr	9	Ti–10Cr [31]
Mo	14	Ti–13Mo [32], Ti–14Mo [33]
V	20	Ti–16V [32], Ti–20V [34]
W	25	
Sn	27	Ti–3Mo–6Sn–8Zr at%, Ti–3Mo–6.5Sn–8Zr at% [35]
Nb	43	Ti–40Nb, Ti–43Nb [36]
Ta	75	Ti–72Ta [37]
Zr	90	Ti–3Mo–7Sn–4Zr at%, Ti–3Mo–7Sn–5Zr at% [35]
Al	−18	Ti–15–Mo–5Zr, Ti–15Mo–5Zr–3Al [34]

$$[Fe]_{eq} = 3.5 \cdot \left(\frac{[Fe]}{3.5} + \frac{[Cr]}{9} + \frac{[Mo]}{14} + \frac{[V]}{20} + \frac{[W]}{25} + \frac{[Sn]}{27} + \frac{[Nb]}{43} + \frac{[Ta]}{75} + \frac{[Zr]}{90} - \frac{[Al]}{18} \right)_{(wt\%)} \quad (20)$$

Identifying TRIP and superelastic alloys

When martensite transformation is induced by an external work, the product phase can either remain or reverse to β after unloading. The first case corresponds to TRIP alloys, the second to superelastic alloys. Once the alloys that cannot form martensite under stress are identified via an $[Fe]_{eq}$ below 3.5 wt%, the M_s^* computation can separate superelastic from TRIP alloys (Fig. 9). If the M_s^* exceeds 90 °C, it is likely that the martensite reverse temperature is above room temperature; once the nucleation is triggered by an external work, martensite is expected to form and to remain after unloading. Thus, these alloys are expected to display TRIP. If $-90\ °C < M_s^* < 90\ °C$, the energy provided by the external stress may enable the growth of the martensite, but its stability at room temperature is not sufficient to remain once the load is removed. Thus, the alloys with $-90\ °C < M_s^* < 90\ °C$ are expected to display superelasticity. If $M_s < -90\ °C$, it is unlikely that the external stress provides enough work for the martensite to grow. Thus, the alloys with $M_s^* < -90\ °C$ are expected to display slip or twinning only. Therefore, combined with the $[Fe]_{eq}$ criterion, the M_s^* calculation allows to predict the type of deformation behaviour of β alloys.

Regions in M_s^* -$[Fe]_{eq}$ space identifying systems undergoing slip or twinning, TRIP or superelasticity effects are shown in Fig. 9

4. Criteria for tailored deformation behaviour

The criteria described above can be combined to predict if a composition is likely to display martensite upon quenching, superelasticity, TRIP or Slip/TWIP effect. The prediction procedure is summed up in Fig. 10.

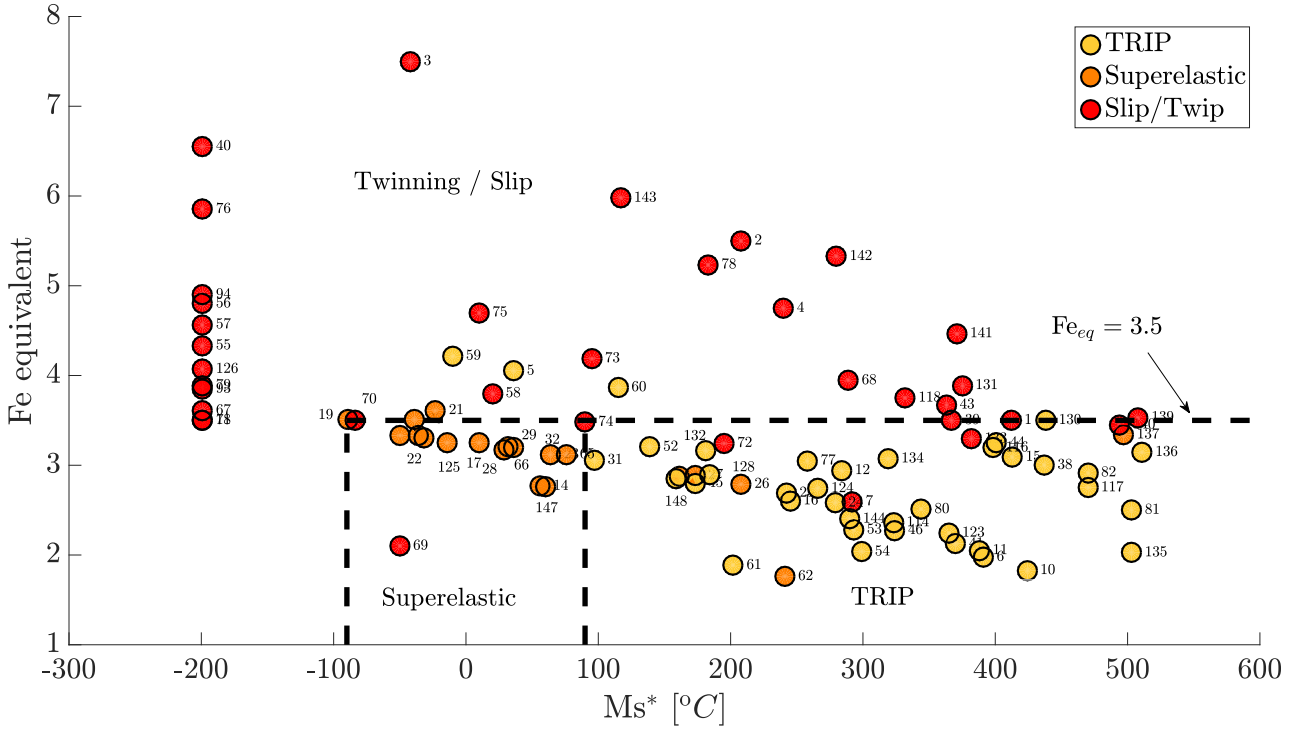

Fig. 9. Map of the alloys from the literature. The three regions corresponding to the indicated deformation behaviour are outlined by the black dotted lines. The colours of the bullets correspond to the experimentally observed behaviour. When the calculations indicated that there was no temperature for which martensite is thermomecanically more stable than β, the M_s^* has been set to −200 °. The number code for each composition is shown in Appendix A. (For interpretation of the references to colour in this figure legend, the reader is referred to the web version of this article.)

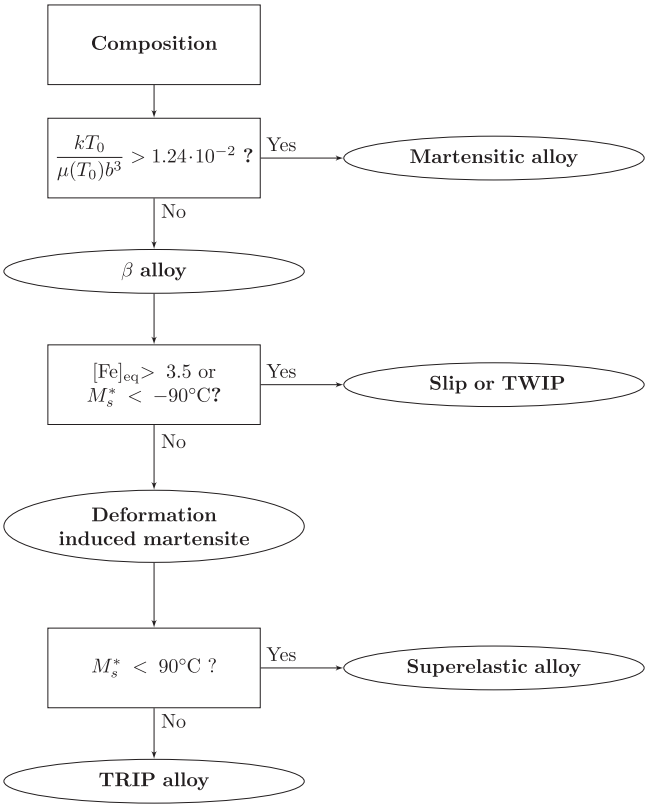

Fig. 10. Suggested procedure to predict the behaviour of titanium alloys as a function of their composition; the value of M_s^* is the one that is calculated according to the procedure described in this article

The performance of the model in discriminating the microstructure at room temperature is displayed in Fig. 6, and the performance in identifying the deformation behaviour of β alloys is shown in Fig. 9.

5. Discussion

5.1. Thermally activated martensite nucleation

To explain why some compositions retain β at room temperature, the assumption of a thermally activated nucleation process seems to be supported by experimental data. Jepson et al. have demonstrated that martensitic transformation can be inhibited in Ti–Nb alloys by quenching at extremely high cooling rates [29]. Their observations are consistent with a thermally activated nucleation mechanism; the higher the cooling rate, the less time is spent at T_0 and the lower is the density number of martensite nuclei (Eq. (18)). This dependency on the cooling rate is expressed in Eq. (19). For a given composition, the nucleation parameter is constant but the critical value for nucleation parameter increases with the quenching rate, which suggests that the martensitic transformation can be inhibited upon quenching if the cooling rate is high enough; this is consistent with Jepson's experimental work [29]. On the other hand, if the energy barrier to martensite nucleation is too high, it may be that the maximal quenching rate that allows martensite nucleation is very low. If it is too low, diffusion can occur during cooling, in such a way that no quenching rate allows martensite formation upon quenching.

Moreover, the common statement according to which β alloys have an M_s below room temperature is not in agreement with experimental observations. For example, the formation of martensite in Ti–10V–2Fe–3Al was investigated by Duerig et al. [16] on six specimens of the same composition. After quenching, one sample showed evidence of martensitic transformation and the five others exhibited a β microstructure at room temperature. These β alloys were cooled down to −170 °C and still exhibited no martensite. During tensile test, however, a critical stress

of around 200 MPa induced martensite transformation that did not reverse to β after unloading. The deformed specimens were then heated and the martensite was found to reverse to β around 200 °C. The variability of the microstructure at room temperature between the different specimens (β or martensite) for this composition is consistent with the proposed nucleation parameter criterion; indeed, for this composition, $kT_0/[\mu(T_0)b^3] = 1.31 \cdot 10^{-2}$ lies very close to the critical threshold of $1.24 \cdot 10^{-2}$. Then, if the M_s temperature was actually below room temperature, it would have to lie below −170 °C. The martensite reverse temperature has been shown by experiment to be around 200 °C, and an M_s below −170 °C would imply a hysteresis of more than 300 °C between the direct and reverse martensite transformation. This is unlikely, since the hysteresis for martensite transformation in titanium alloys typically lies around 10 °C when it can be measured. Other experiments performed on TRIP alloys show that the martensite formed during deformation reverses to β at temperatures exceeding room temperature by more than 100 °C [38,39]. Moreover, isothermal formation of martensite that does not involve any diffusion has been observed in at least three different titanium alloys [40,41]. For these three cases, the temperature at which martensite isothermally formed is below or around the calculated martensite stabilization temperature M_s^*. This supports the statement that martensite formation in titanium alloys is a diffusionless thermally activated process. Therefore, the hypothesis that the martensite stabilisation temperature M_s^* lies above room temperature for TRIP alloys, and that martensite nucleation requires external stress, while growth occurs mainly athermally, seems to be consistent with experimental evidence. The existence of such a transformation, where the nucleation is thermally activated but the growth is athermal, has been reported by Laughlin et al. [42], where it is designated as anisothermal. Cottrell also supports the idea that martensite nucleation is thermally activated [43].

Moreover, this statement allows to explain the difference of behaviour between superelastic and TRIP alloys. It is sometimes believed that the difference between TRIP alloys and superelastic alloys lies in the fact that martensite is somehow stabilized by plastic deformation (or “stress induced”) in TRIP alloys whereas superelasticity is observed when martensite formation occurs before plastic deformation (“strain induced”). However, in TRIP alloys, martensite sometimes forms under stress before plastic deformation occurs, as shown by the characteristic double yielding on the stress–strain curve [44], and still remains upon unloading. This means that plastic deformation is not necessary to stabilise the deformation induced martensite. Conversely, a significant part of the martensite that forms upon deformation in superelastic alloys reverses even in heavily plastically deformed samples [45], which means that plastic deformation alone is not sufficient to explain the stabilisation of deformation induced martensite in the case of TRIP alloys. Therefore, the concomitance between plastic deformation and martensite formation is not necessary to explain the occurrence of TRIP effect. On the other hand, thermodynamic criteria (via M_s^* calculation) allow to separate superelastic from TRIP alloys. In both cases, external work triggers martensite nucleation at room temperature. For superelastic alloys, M_s^* lies around room temperature and M_f lies below room temperature; the martensite is unstable at room temperature, which explains the reversion to β phase upon unloading. For TRIP alloys, M_s^* is far above room temperature, martensite is more stable than β phase at room temperature, and once the transformation is triggered, most of it remains and is unable to reverse to β upon unloading.

5.2. Role of the ω phase

The stabilisation of β phase is often attributed to athermal ω phase [18,46], which formation during quenching would occur above M_s and inhibit the martensitic transformation [18]. Assuming that ω phase forms at temperatures above or around M_s during cooling, it would indeed be likely that martensite formation is inhibited, due to a competition between both phases [46]. However, the idea that ω phase systematically forms above M_s in alloys that retain β phase upon quenching is not supported by thermodynamic calculations. The thermodynamic database ‘TCTI1’ of Thermo-Calc® has been used to compute, for alloys from literature, the temperature T_0^ω at which ω phase and β phase exhibit the same free energy. T_0^ω is expected to be the highest temperature at which ω transformation can possibly occur upon quenching. For most alloys experimentally known to retain β phase at room temperature, the computed T_0^ω was lower than the calculated M_s^*. This suggests that the ω phase nucleates below the temperature at which martensite should have formed, and that the absence of martensite cannot be attributed to the prior presence of ω. Moreover, it has been shown that martensite and ω phase can coexist at room temperature after quenching, and that the ω particles could transform to β upon deformation, before further transforming into martensite [47]; implying that the presence of ω is not necessarily an obstacle to martensite formation. Therefore, although it certainly plays a role in the deformation behaviour of titanium alloys, it seems that the competition between ω and martensite is not necessary to explain the retention of β at room temperature. The nucleation parameter proposed in this work, on the other hand, suggests an explanation for β retention, quantitatively supported by calculations and qualitatively consistent with experimental evidence.

5.3. M_s prediction

The martensite stabilisation temperature M_s^*, which is the highest temperature at which martensite is observed if nucleation is possible, shows good agreement with experimental measurements of M_s, as can be seen in Fig. 5. However, it should be noted that among the 54 compositions that are displayed in Fig. 5, 43 correspond to binary alloys and 11 to multicomponent alloys, because limited information is available on the M_s of quenched multicomponent alloys[4]. The model for the M_s^* temperature does not work well for alloys containing a significant concentration of tin (Fig. 5). The reason for this is not clear. Other M_s models that include tin also had difficulties with such alloys ([18]).

In binary systems, the martensite generally has an HCP structure until a critical composition at which the transition to orthorhombic structure occurs. The M_s^* calculation is performed by assimilating the free energy of the orthorhombic phase to the one of the HCP phase. Yan and Olson made this assumption before, and justified it by the continuity of the M_s temperature at the HCP/orthorhombic transition composition [18]. In the present M_s^* calculation, although the difference between orthorhombic and HCP phase cannot be considered when performing thermodynamic computation, it is taken into account in the calculation of the elastic strain energy. Some authors have empirically calibrated the value of the free energy in order to account for the difference between free energies of the HCP phase and the orthorhombic phase [18]. Since good agreement between experimental and calculated values is obtained with the model proposed here (Fig. 5), which is free of fitting parameters, we suggest that it is reasonable to approximate the free energy of α'' by the one of α'.

Several attempts have been made to predict the M_s temperature in Titanium alloys. Galindo-Nava suggested a model free of fitting parameters to calculate the M_s temperature in binary alloys, but it does not consider multicomponent alloys [21], and mainly focuses on high temperatures. Neelakantan et al. [48] as well as Yan [18] proposed an approach based on Ghosh and Olson’s theory [49]. These two models provided good results. However, they did not calculate the elastic strain energy, but used instead a linear function of the atomic fractions of the alloying elements, supposed to include both elastic strain energy and frictional work, and fitted from experimental data. In the present work, the calculated M_s^* is the temperature at which the energy of a martensite plate

[4] M_s is sometimes estimated while applying a low stress during cooling (for example 50 MPa in [37]). The M_s measurements obtained with indirect methods are not displayed in Fig. 5

of detectable size reaches a local minimum (Eq. (12)). This minimum of energy, by definition, does not depend on the work dissipated during the transition from one state to the other, and there is thus no need to compute any work related to internal friction to determine M_s^* as it is defined here. If frictional work that opposes the transformation is to be considered in the model, it should be included both during growth and nucleation under the form of an energy barrier. In the case of martensite induced upon quenching, the main source of energy to overcome the nucleation barrier is thermal. As martensite growth is very fast, it cannot be assumed that growth requires significant thermal activation. Thus, if some frictional work opposes martensite growth, its magnitude has to be smaller than the nucleation barrier, in such a way that overcoming the nucleation energy barrier by thermal energy allows to overcome the energy barrier for martensite growth as well. Since the energy barrier for nucleation is not explicitly calculated in this work, the proposed nucleation parameter obtained by collective fitting already incorporates the effect of frictional work.

The computation of M_s^* takes into account the grain size effect Eq. (12). Note that the calculations were performed by assuming a grain size of 100 μm. As long as the grain size is in the range 20–100 μm, the M_s^* calculation was found not to be very sensitive to grain size; the maximal difference between the M_s^* calculated for 20 μm and the one for calculated for 100 μm was 30 °C. The M_s^* strongly varies with grain size only for smaller grains. M_s^* decreases when the grain size is reduced, because the elastic strain energy increases. The decreasing of the M_s with decreasing grain size has been confirmed in steels [50,51]. This grain size dependency suggests that martensite growth becomes more and more difficult if the microstructure is refined. In particular, if twinning occurs in conjunction with martensite nucleation, the free path for martensite radial growth (see Fig. 2b) can be considerably diminished. In the β grains containing twins, the M_s^* can therefore be dramatically decreased. For example, in the case of Ti–12Mo, the M_s^* for a standard grain size of 100 μm is 437 °C and stable plates of martensite are expected to form upon deformation (which is consistent with experiments; TRIP effect is displayed in this alloy [22]). If multiple twins nucleate in a grain, reducing the apparent grain size to, say, 600 nm, the M_s^* falls to 1 °C. With such a value of M_s^*, any plate of martensite that would form between or inside the twins would be expected to reverse upon unloading. This might help explaining why in TRIP/TWIP alloys, the microstructure after deformation often consists of a mixture of β and martensite, and not of 100% martensite, despite a sometimes very high M_s^*. In alloys displaying both TRIP and TWIP, a limited amount of martensite has already been reported to reverse to β upon unloading, even though most of the martensite remained after deformation [22,52]. This seems to be consistent with the grain size dependency advanced here.

In the end, the proposed model for M_s^* provides a rather accurate prediction of M_s over a wide range of compositions and alloys, while being physically-based and using minimal fitting as opposed to most existing models. Fig. 5 is obtained without any adjustable parameter, and the only data-derived parameter is the threshold value of the nucleation parameter $\frac{kT_0}{\mu(T_0)b^3}$ from Fig. 6 to account for thermally activated nucleation.

5.4. Comparison with usual design tools

Microstructure prediction

The type of microstructure formed at room temperature can be predicted with good accuracy: martensitic multicomponent alloys can be identified, as shown in Fig. 6. Moreover, the proposed nucleation parameter criterion ($kT_0/[\mu(T_0)b^3]$) seems to be a physically relevant indicator since it allows to predict for each binary system the critical composition necessary to retain β at room temperature, as shown in Fig. 8 and Table 1. The criterion that is used in the literature to predict the possibility to retain β at room temperature is the "molybdenum equivalent" ($[Mo]_{eq}$) [26] calculated as follows:

$$[Mo]_{eq} = [Mo] + 0.67[V] + 0.44[W] + 0.28[Nb] + 0.22[Ta] + 1.6[Cr] + 1.25[Ni] + 1.7[Co] + 2.9[Fe] - 1.0[Al](wt.\%) \quad (21)$$

The coefficients to the concentrations in the $[Mo]_{eq}$ calculation have been established in the following way: for each alloying element, the critical concentration to retain β at room temperature in the Ti–Mo system (10 wt%) is divided by the critical concentration (experimentally observed) necessary to retain β at room temperature for the given element. It is generally accepted that an alloy can retain β at room temperature if $[Mo]_{eq}$ is greater than 10%.

For binary alloys, both criteria ($[Mo]_{eq}$ and the nucleation parameter) - Inequation (19) give similar (and correct) results. However, the equation of the $[Mo]_{eq}$ has been defined so as to provide correct results for binary alloys, so the challenge remains on the prediction for multicomponent alloys. For those, the nucleation parameter criterion may present an advantage. The microstructure prediction is successful for 92% of the alloys with the nucleation parameter method, and for 88% of the alloys with the $[Mo]_{eq}$ method. The nucleation parameter criterion also integrates the effect of Zr and Sn, absent in the $[Mo]_{eq}$. Consequently, although the $[Mo]_{eq}$ is a reliable tool to predict the microstructure, the nucleation parameter presents the advantages of offering a physical explanation for the β retention, of allowing more accurate predictions and of being applicable to a more diverse palette of elements.

Deformation behaviour prediction

The deformation behaviour of β alloys can be fairly well predicted as well. The method presented in Fig. 9 to categorize the different β alloys gives reasonable trends. Two compositions have M_s^* >90 °C and still display superelasticity (Ti–31Nb–9Zr at % and Ti–3Mo–10Zr-–5.5Sn at %). Both of them have a high concentration in Zr, and the M_s^* may be mispredicted because of a wrong estimation of the influence of Zr on the lattice parameters. For most of the other wrong predictions, the compositions involved are close from the borders defined by the threshold.

Regarding the retention of β upon deformation, the proposed $[Fe]_{eq}$ assumes that the effect of each alloying element in multicomponent systems can be extrapolated from its individual effect in binary systems. It is built in a similar way to the $[Mo]_{eq}$, but while the $[Mo]_{eq}$ equation is established with the critical concentrations necessary to retain β upon quenching in binary alloys, the proposed $[Fe]_{eq}$ is based on the critical concentrations necessary to retain β upon deformation. Two elements that are not included in the $[Mo]_{eq}$ equation, Zr and Sn, are taken into account in the $[Fe]_{eq}$ criterion. These two elements are often considered to be neutral with respect to the β stability, because they have little influence on the β transus temperature. However, it has been experimentally shown in [35] that the concentration in Zr and Sn significantly influences the deformation behaviour of β titanium alloys.

The method presented here offers a new approach for designing martensitic, TRIP, or superelastic alloys, differing from the traditional Bo–Md method [10]. To discuss its accuracy, literature data collected for this work is gathered on a Bo–Md map (Fig. 1b). The corresponding zones are displayed in Fig. 1a. It can be seen that the boundary between martensitic and non martensitic alloys is relatively well predicted by Morinaga's map, and that most of the alloys displaying TRIP are indeed in the "TRIP–TWIP" zone. However, an appreciable quantity of martensitic alloys are in the predicted TRIP–TWIP zone, some TRIP alloys are outside the TRIP–TWIP zone, and so the boundaries do not seem to describe very accurately the deformation behaviour. Moreover, the significant number of TWIP alloys in the Slip zone does not support the idea that a clear zone separates TWIP from slip (65% of the alloys from Appendix A known to display TWIP are not in the TRIP–TWIP zone of the Bo–Md map). Additionally, as discussed above, the

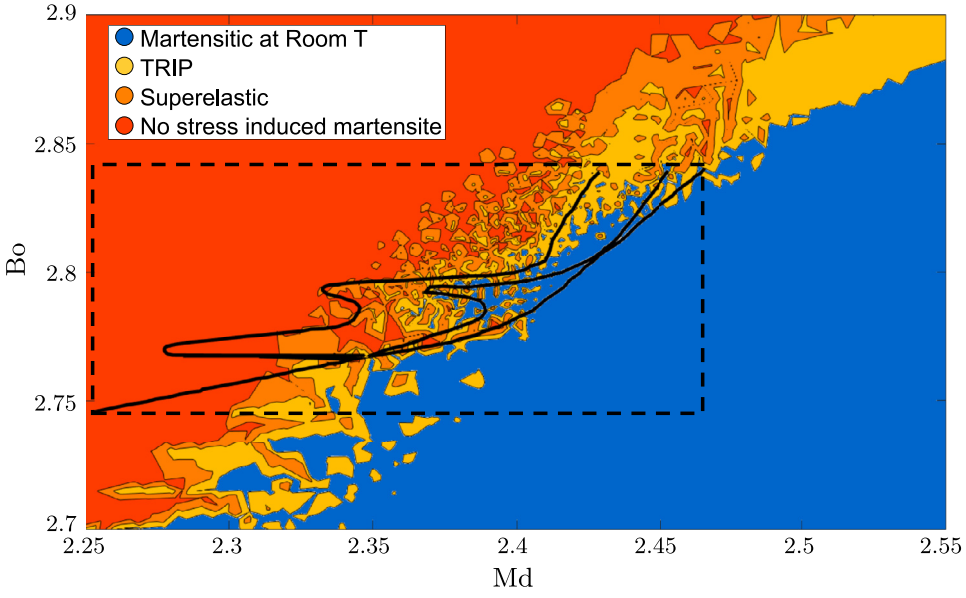

Fig. 11. Expected behaviour as a function of the Bo and Md parameters, according to the method described in this work. Morinaga's map has been superimposed to the chart (plain lines) for comparison purpose; the behaviour expected in the zones delimited by black lines, according to Morinaga's map, is displayed in Fig. 1a.

statement that the boundary between TRIP and martensitic alloys is defined by the equation M_s = Room Temperature (RT) is questionable, so it should not be assumed that the M_s is constant on the line displayed as "M_s=RT" in Fig. 1a. The lines separating the types of behaviour have been drawn with existing alloys, and no physical background justifies the peculiar shape obtained.

The method proposed in this work on the other hand, is semi-empirical, meaning that it uses empirical thresholds with models that rely on physical bases (for M_s^* and the nucleation parameter). The quantities to be calculated in order to predict the behaviour can be computed with a simple code that runs efficiently. Although the method does not rely entirely on physics, it gives some leads to better understand the composition dependency of martensite formation, and allows to predict with good confidence the behaviour of the alloys, as can be seen in Fig. 9 and Fig. 6. It offers advantages compared to the current methods. The composition space to be explored is not limited by the Bo–Md combinations defined by the frame of the map (Fig. 1a) and a criterion is proposed to target superelasticity. In order to compare the predictions obtained with the stability map with the ones obtained with the present work, the method described here has been applied to a set of approximately 6000 compositions chosen in such a way that they fill the space of the Bo–Md map. The corresponding predictions are displayed in Fig. 11. The overall shape of the martensitic zone is roughly similar to the one of the phase stability map of [10] (Fig. 1a), but according to the present calculation method, there should be many TRIP regions in the middle of the martensite area. The regions corresponding to the different deformation mechanisms assessed with the method presented here are very scattered in the Bo–Md space; this suggests that the values of Bo and Md may not be the most physically relevant parameters to describe the deformation induced transformations in titanium alloys. The method proposed in this work can be used to design TRIP/TWIP alloys; it is capable to determine the compositional dependence of TRIP and superelasticity effects. It may constitute a useful tool to design β titanium alloys exploring novel ranges of composition.

6. Conclusion

A new model is proposed to describe the martensitic transformation in titanium alloys - either upon quenching or deformation - as a function of their composition. Although it uses *ad hoc* thresholds and one empirical criterion ($[Fe]_{eq}$), the proposed model relies on physical approaches to determine martensite nucleation and growth. The nucleation parameter ($kT_0/[\mu(T_0)b^3]$) allows to determine the type of microstructure present at room temperature, the $[Fe]_{eq}$ and M_s^* criteria then allow to identify the deformation behaviour of the β alloys. When $kT_0/[\mu(T_0)b^3] > 1.24 \cdot 10^{-2}$, martensite is expected to form upon quenching. Otherwise, the alloy retains β at room temperature. If the alloy displays only β phase at room temperature, it deforms by slip or twinning if $[Fe]_{eq} > 3.5$ or if $M_s^* < -90$ °C, whereas it can form martensite upon deformation otherwise. Among the alloys that can form martensite upon deformation, superelasticity is expected if -90 °C $< M_s^* < 90$ °C, whereas TRIP is expected if $M_s^* > 90$ °C.

This approach can provide explanations for some characteristic features of titanium alloys that had not quantitatively been modeled so far. The assumption of a thermally activated martensite nucleation may explain why some alloying elements allow to retain the β phase at room temperature. The determination of a more precise expression for the energy barrier to martensite nucleation could constitute the focus of some future work. The M_s^* model relies on thermodynamics and micromechanics and offers an explanation for the composition dependence of TRIP and superelastic effects. The combination of these models allows to discriminate martensitic, TRIP, superelastic and TWIP/Slip alloys and may be used as a designing tool for tailored deformation behaviour.

Declaration of interests

The authors declare that they have no known competing financial interests or personal relationships that could have appeared to influence the work reported in this paper.

Acknowledgment

The work of MB has been supported by DGA (French Ministry of Defense). PEJRDDC is grateful to the Engineering and Physical Sciences Research Council EPSRChttps://doi.org/10.13039/501100000266.K. for the provision of funding via grant EP/L025213/1 (Designing Alloys for Resource Efficiency), and to the Royal Academy of Engineering for funding his chair.

Appendix A. Alloys from the literature

n	Alloy composition (w %)[a]	Microstructure	Ms	Deformation mechanism	Ref
1	Ti–10Mo–1Fe	β		TWIP {332}	[30]
2	Ti–10Mo–3Fe	β		Slip	[53]
3	Ti–10Mo–5Fe	β		Slip	[53]
4	Ti–15Mo–1Fe	β		Slip	[54]
5	Ti–10V–3Fe–3Al–0.27O	β		TRIP TWIP {332} stress-induced ω	[55]
6	Ti–8Mo–4Nb–2V–3Al	β		TRIP	[56] [57]
7	Ti–9.6Mo–4Nb–2V–3Al–0.25Fe	β		Apparently no TRIP	[56]
8	Ti–11Mo–4Nb–2V–3Al	β		No information	[56]
9	Ti–29Nb–13Ta–4.6Zr	β		?	[58]
10	Ti–10V–2Cr–3Al	β and a bit of α''	?	TRIP	[59]
11	Ti–10V–1Fe–3Al	β and a bit of α''		TRIP	[59]
12	Ti–3Al–5Mo–7V–3Cr	β		TRIP TWIP {332}	[60]
13	Ti–31Nb–9Zr	β		Superelastic (grain size 1μm)	[61]
14	Ti–38Nb–1.4Al	β		Superelastic	[62]
15	Ti–9Mo–6W	β		TRIP TWIP {332} stress-induced ω	[11]
16	Ti–32Nb	β [27] or α'' [36]		TRIP	[36] [63] [27]
17	Ti–40Nb	β		Superelastic	[36]
18	Ti–43Nb	β		Slip	[36]
19	Ti–2Mo–37Nb			Superelastic	[36]
20	Ti–3.3Mo–33Nb			Superelastic	[36]
21	Ti–5Mo–29Nb			Superelastic	[36]
22	Ti–30Nb–19Ta			Superelastic	[36]
23	Ti–34Nb–9Zr			Superelastic	[36]
24	Ti–15Nb–12Zr at %	β			[64]
25	Ti–16Nb–12Zr at %	β			[64]
26	Ti–17Nb–12Zr at %	β		Superelastic TRIP?	[64]
27	Ti–18Nb–12Zr at %	β		Superelastic	[64]
28	Ti–19Nb–10Ta at %	β		Superelastic	[64]
29	Ti–12Nb–20Ta at %	β		Partial superelasticity	[64]
30	Ti–13Nb–20Ta at %	β		Partial superelasticity	[64]
31	Ti–62Ta–2Nb	β		TRIP	[64]
32	Ti–61Ta–4Nb	β		Superelastic	[64]
33	Ti–2Mo	α'	780		[65]
34	Ti–3Mo	α'	740		[65]
35	Ti–4Mo	α'	700		[65]
36	Ti–6Mo	α''	610		[65]
37	Ti–8Mo	α''	515		[65]
38	Ti–12Mo	β		TRIP TWIP ({332} and {112})	[33]
39	Ti–14Mo	β		pure TWIP	[33]
40	Ti–13V–11Cr	β		Slip	[66]
41	Ti–5Al–5Mo–5V–3Cr	β		TRIP	[67]
42	Ti–5Mo–6V–3Cr–3Al	β		TWIP{112} and {332} No information regarding TRIP	[68]
43	Ti–11.5Mo–6Zr–4.5Sn	β (quenched -195°C))		TWIP {112} and{332}	[34] [15]
44	Ti–13Mo	β		TRIP	[32]
45	Ti–16V	β		TRIP TWIP stress-induced ω	[32] [69]
46	Ti–13V	β [38] or α'' [28]		TRIP[38]	[28,38]
47	Ti–4Al–9V–1.2Fe	α''	483		[18]
48	Ti–3.2Al–14.6V	α''	493		[18]
49	Ti–15.15V–3.17Al	α''	463		[18]
50	Ti–15.6V–3.1Al	α''	423		[18]
51	Ti–13V-3A–0.6Fe	α''	453		[18]
52	Ti–13V–3Al–1Fe at	β + a bit of α''		TRIP	[39]
53	Ti–13V–1Al at	β + α''			[38]

(continued on next page)

[a] unless "at% is mentioned

(*continued*)

n	Alloy composition (w %)[a]	Microstructure	Ms	Deformation mechanism	Ref
54	Ti–13V–3Al at	β + α''	over 350		[18,39]
55	Ti–16V–2Fe–2Al	β		Slip	[70]
56	Ti–16V–2Fe	β		Slip	[70]
57	Ti–16V–2Fe–Al	β		Slip	[70]
58	Ti–16V–Fe	β		TWIP {332} stress-induced ω	[70]
59	Ti–14V–2Fe–Al	β		TWIP {332} mainly detection of stress-induced α''	[70]
60	Ti-12V-2Fe-Al	β		TWIP {332} mainly detection of stress-induced α''	[70]
61	Ti-16.1V-4Al	β		TRIP	[39] [71]
62	Ti-15.4V-4Al	β + ordered α''			[71]
63	Ti-13V-3Al-1.5Fe at	β		?	[39]
64	Ti-13V-3Al-0.5Fe at	mainly α''	$A_s = 240$ $A_f = 281$ $M_s \approx 250$?		[39]
65	Ti-25Ta-25Nb	β		Superelastic	[72]
66	Ti-25Ta-24Nb	β		Superelastic TWIP ({332} and {112})	[3] [73]
67	Ti-25Ta-30Nb	β		TWIP {332}	[73]
68	Ti-15Mo-5Zr	β		TWIP {332}	[34]
69	Ti-20V-6Al	β		Slip	[34]
70	Ti-20V	β		TWIP {332}	[34]
71	Ti-20V-0.15O	β		TWIP {332}	[66]
72	Ti-15Mo-5Zr-3Al	β		Slip	[34]
73	Ti-3Al-8V-6Cr-4Mo-4Zr	β		Slip	[34]
74	Ti-15V-3Cr-3Al-3Sn	β		Slip	[34]
75	Ti-8Mo-8V-2Fe-3Al	β		Slip	[34]
76	Ti-13V-11Cr-3Al	β		Slip	[34] [10]
77	Ti-10V-2Fe-3Al	β or α'' + β		TRIP	[16]
78	Ti-12Mo-6Zr-2Fe	β		TWIP	[10]
79	Ti-20V-3Sn	β		TWIP	[34]
80	Ti-4Al-7Mo-3V-3Cr	β		TRIP TWIP	[74]
81	Ti-10Mo	β + α'' (segregation)		TWIP {332} (+TRIP?)	[53]
82	Ti-7Mo-3Cr	β		TRIP TWIP{332} and {112}	[12]
83	Ti-1Cr	α'	800		[28]
84	Ti-2Cr	α'	750		[28]
85	Ti-3Cr	α'	700		[28]
86	Ti-3.5Cr	α'	650		[28]
87	Ti-4.2Cr	α'	620		[28]
88	Ti-1.91V	α'	807		[28]
89	Ti-4.24V	α	727		[28]
90	Ti-6.9V	α	627		[28]
91	Ti-8.5V	α	527		[28]
92	Ti-12.7V	α	327		[28]
93	Ti-22V	β		TWIP {112}	[75]
94	Ti-28V	β		TWIP {112}	[75]
95	Ti-2.9Al	α	918		[29]
96	Ti-5.9Al	α	960		[29]
97	Ti-9Al	α	1015		[29]
98	Ti-12.3Al	α	1060		[29]
99	Ti-1Fe	α	760		[28]
100	Ti-2Fe	α	675		[28]
101	Ti-2.5Fe	α	630		[28]
102	Ti-3Fe	α	575		[28]
103	Ti-4Fe	α	475		[28]
104	Ti-12W		660		[28]
105	Ti-18W		480		[28]
106	Ti-21.9W		350		[28]
107	Ti-9.1Nb		759		[29] [48]
108	Ti-10Nb		720		[29,48]
109	Ti-13Nb		680		[29] [48]
110	Ti-14Nb		650		[29,48]
111	Ti-17Nb		578		[29,48]
112	Ti-22Nb		485		[29] [48]
113	Ti-25Nb		387		[29,48]
114	Ti-29Nb	β or α''	307		[29,48]
115	Ti		855		[29] [28]
116	Ti-12Mo-5Zr	β		TRIP TWIP {332}	[76]
117	Ti-11Mo	α'' [77] or β			[29]

(*continued on next page*)

(*continued*)

n	Alloy composition (w %)[a]	Microstructure	Ms	Deformation mechanism	Ref
118	Ti-15Mo	β		TWIP {332}	[54]
119	Ti-10Zr		777		[48]
120	Ti-17.5Zr		727		[48]
121	Ti-24.42Zr		652		[48]
122	Ti-32.52Zr		627		[48]
123	Ti-25Nb-2Ta-3Zr	β		TRIP	[78]
124	Ti-25Nb-10Ta-1Zr-0.2Fe	β		TRIP	[78]
125	Ti-38Nb-3Zr-2.1Ta	β		Superelastic[b] TWIP 332	[79]
126	Ti-50Nb	β		TWIP {112} stress-induced ω	[80]
127	Ti-15Ta	α	760		[29]
128	Ti-62Ta	α'' or β		stress-induced Martensite[c]	[37] [81]
129	Ti-72Ta	β		stress-induced Martensite[d]	[37]
130	Ti-8.5Cr-4.5Sn	β		TRIP TWIP {332}	[82]
131	Ti-10Cr	β		TWIP {332}	[31]
132	Ti-25Nb-3Zr-3Mo-2Sn	β		TWIP {332} mainly TWIP {112} TRIP stress-induced ω	[83]
133	Ti-6Cr-4Mo-2Al-2Sn-1Zr	β		TWIP {332} TWIP {112} stress-induced ω	[84]
134	Ti-10V-4Cr-1Al	β		TWIP {332} TWIP {112} TRIP (unstable)	[52]
135	Ti-5Al-2Sn-4Zr-4Mo-2Cr-1Fe	β		TRIP	[85]
136	Ti-3Mo-8Zr-5Sn at%	β		TRIP	[35]
137	Ti-3Mo-9Zr-5.5Sn at%	β		Superelastic	[35]
138	Ti-3Mo-5Zr-4Sn at%	α''			[35]
139	Ti-3Mo-6Zr-7Sn at%	β		Slip	[35]
140	Ti-3Mo-10Zr-6Sn at%	β		Slip	[35]
141	Ti-10Ta-4Fe	β		Slip	[86]
142	Ti-7Ta-5Fe	β		Slip	[86]
143	Ti-12Nb-5Fe	β		Slip	[86]
144	Ti-13V at	β		TRIP	[38]
145	Ti-16Nb-4Sn at	$\beta + \alpha''$	87		[87]
146	Ti-16Nb-5Sn at	$\beta + \alpha''$	−53		[87]
147	Ti-24Nb-3Al at	mainly β	−13	superelastic	[62]
148	Ti-35Nb	β or α''	175	TRIP	[88] [89]
149	Ti-35Nb-3Sn	α''	77		[88]

Appendix B. Composition dependence of the lattice parameters

When the composition dependency was not found in the literature, the effect of the alloying element was either ignored or obtained by extrapolation (like the effect of Zr and Sn in the orthorhombic phase). x_i is the atomic fraction of element *i*.

BCC (V, Mo, Fe, Cr from [27], Nb from [14], Zr and Sn from [35]) :

$$a_\beta = 3.274 + 0.043x_{Nb} - 0.1259x_{Mo} - 0.2x_V - 0.55x_{Fe} - 0.15x_W + 0.044x_{Ta} + 0.11x_{Sn} - 0.4x_{Cr} + 0.31x_{Zr}\text{Å}$$

HCP (Zr from [90], Mo, Nb, Ta from [91], V, W, Fe from [92], Cr from [93]):

$$a_{\alpha'} = 2.959 - 0.083x_{Fe} - 1.3x_W + 0.22x_{Zr} - 0.26x_{Cr} - x_V\text{Å}$$
$$b_{\alpha'} = \sqrt{3}a_{\alpha'}\text{Å}$$
$$c_{\alpha'} = 4.68 + 0.2381x_{Mo} + 0.5x_{Nb} + 0.5x_{Ta} - 0.4x_W - 0.4x_V + 0.1x_{Fe} + 0.5x_{Zr} - 1.6x_{Cr}\text{Å}$$

Orthorhombic (Zr and Sn from [35], Ta and Nb from [73], Mo from [91], V, W from [92], Cr extrapolated from [67]), Fe and Al extrapolated from[18]:

$$a_{\alpha''} = 2.89 + 1.37x_{Nb} + 3x_{Mo} + 0.6x_{Ta} + 2.43x_W + 2.05x_{Sn} + x_V + 3x_{Cr} + 0.9x_{Zr} + 0.083x_{Al} + 0.0223x_{Fe}\text{Å}$$
$$b_{\alpha''} = 3.02\sqrt{3} - 1.68\sqrt{3}x_{Nb} - 3\sqrt{3}x_{Mo} - 1.21x_{Ta} - 1.42\sqrt{3}x_W - 2.64x_{Sn} - 0.28x_{Zr} - \sqrt{3}x_V - 5.67x_{Cr} - 0.018x_{Al} + 0.0504x_{Fe}\text{Å}$$
$$c_{\alpha''} = 4.734 - 0.184x_{Nb} - 1.5x_{Mo} - 0.4x_{Ta} - 0.57x_W + 0.23x_{Sn} + 0.4x_V - 2.67x_{Cr} + 0.3x_{Zr} - 0.0535x_{Al} - 0.0326x_{Fe}\text{Å}$$

As explained in the text, in order to compute M_s, the elastic energy was calculated both for the HCP and for the orthorhombic structure, by assuming that the composition dependence of the lattice parameters for each structure can be extrapolated in domains where they do not exist. For each alloy, two M_s were obtained (one for each structure) and the retained one was the greatest of both. For all binary systems except for Ti–V, this extrapolation of the lattice parameters allowed to find the critical composition at which the transition from HCP to orthorhombic happens. For alloys containing Vanadium however, the extrapolation of the composition dependency of the lattice parameters of the HCP structure in domains where this structure does not exist (V>6% at [92]) did not allow to find the critical composition where orthorhombic structure

[b] The alloy is not referred to as superelastic in [79] but after unloading, many martensite plates reverse to β.

[c] no information on whether it is TRIP or superelastic (most likely TRIP).

[d] no information on whether it is TRIP or superelastic.

is more favourable than HCP structure. It seems that the extrapolation of the lattice parameters of the HCP structure is not valid in this system. Thus, for alloys containing more than 6% at of vanadium, the calculations are performed by considering that the lattice parameters of the martensite are those of the orthorhombic structure.

References

[1] G.G. Lütjering, J.C.J.C. Williams, Titanium, Springer, 2003.
[2] Y. Tanaka, Y. Himuro, R. Kainuma, Y. Sutou, T. Omori, K. Ishida, R. Kainuma, K. Ishida, Ferrous polycrystalline shape-memory alloy showing huge superelasticity, Science 327 (5972) (2010) 1488–1490, doi:10.1126/science.1183169.
[3] E. Bertrand, P. Castany, I. Péron, T. Gloriant, Twinning system selection in a metastable β-titanium alloy by Schmid factor analysis, Scr. Mater. 64 (12) (2011) 1110–1113, doi:10.1016/j.scriptamat.2011.02.033.
[4] D.J. Fernandes, R.V. Peres, A.M. Mendes, C.N. Elias, Understanding the shape-memory alloys used in orthodontics., ISRN Dent. 2011 (2011) 132408, doi:10.5402/2011/132408.
[5] G. Song, N. Ma, H.-N. Li, Applications of shape memory alloys in civil structures, Eng. Struct. 28 (9) (2006) 1266–1274, doi:10.1016/J.ENGSTRUCT.2005.12.010.
[6] M.M. Kheirikhah, S. Rabiee, M.E. Edalat, in: A Review of Shape Memory Alloy Actuators in Robotics, Springer, Berlin, Heidelberg, 2011, pp. 206–217, doi:10.1007/978-3-642-20217-9_s8.
[7] B. Sun, X. Meng, Z. Gao, W. Cai, Martensite structure and mechanical property of Ti–Nb–Ag shape memory alloys for biomedical applications, Vacuum 156 (2018) 181–186, doi:10.1016/J.VACUUM.2018.07.029.
[8] F. Sun, J. Zhang, C. Brozek, M. Marteleur, M. Veron, E. Rauch, T. Gloriant, P. Vermaut, C. Curfs, P. Jacques, F. Prima, The role of stress induced martensite in ductile metastable beta Ti-alloys showing combined TRIP/TWIP effects, Mater. Today: Proc. 2 (2015) S505–S510, doi:10.1016/J.MATPR.2015.07.336.
[9] R.P. Kolli, W.J. Joost, S. Ankem, Phase stability and stress-induced transformations in beta titanium alloys, JOM 67 (6) (2015) 1273–1280, doi:10.1007/s11837-015-1411-y.
[10] D. Kuroda, M. Niinomi, M. Morinaga, Y. Kato, T. Yashiro, Design and mechanical properties of new β type titanium alloys for implant materials, Mater. Sci. Eng.: A 243 (1–2) (1998) 244–249, doi:10.1016/S0921-5093(97)00808-3.
[11] F. Sun, J. Zhang, M. Marteleur, C. Brozek, E. Rauch, M. Veron, P. Vermaut, P. Jacques, F. Prima, A new titanium alloy with a combination of high strength, high strain hardening and improved ductility, Scr. Mater. 94 (2015) 17–20, doi:10.1016/J.SCRIPTAMAT.2014.09.005.
[12] J. Gao, Y. Huang, D. Guan, A.J. Knowles, L. Ma, D. Dye, W.M. Rainforth, Deformation mechanisms in a metastable beta titanium twinning induced plasticity alloy with high yield strength and high strain hardening rate, Acta Mater. 152 (2018) 301–314, doi:10.1016/J.ACTAMAT.2018.04.035.
[13] L. Lilensten, Y. Danard, C. Brozek, S. Mantri, P. Castany, T. Gloriant, P. Vermaut, F. Sun, R. Banerjee, F. Prima, On the heterogeneous nature of deformation in a strain-transformable beta metastable Ti–V–Cr–Al alloy, Acta Mater. 162 (2019) 268–276, doi:10.1016/j.actamat.2018.10.003.
[14] M. Bönisch, T. Waitz, M. Calin, W. Skrotzki, J. Eckert, Tailoring the Bain strain of martensitic transformations in TiNb alloys by controlling the Nb content, Int. J. Plast. 85 (85) (2016) 190–202, doi:10.1016/j.ijplas.2016.07.010.
[15] H. Rack, D. Kalish, K. Fike, Stability of as-quenched beta-III titanium alloy, Mater. Sci. Eng. 6 (3) (1970) 181–198, doi:10.1016/0025-5416(70)90048-0.
[16] T. Duerig, J. Albrecht, D. Richter, P. Fischer, Formation and reversion of stress induced martensite in Ti–10V–2Fe–3Al, Acta Metall. 30 (12) (1982) 2161–2172, doi:10.1016/0001-6160(82)90137-7.
[17] P. Wollants, J. Roos, L. Delaey, Thermally- and stress-induced thermoelastic martensitic transformations in the reference frame of equilibrium thermodynamics, Progr. Mater. Sci. 37 (3) (1993) 227–288, doi:10.1016/0079-6425(93)90005-6.
[18] J.-Y. Yan, G. Olson, Computational thermodynamics and kinetics of displacive transformations in titanium-based alloys, J. Alloys Compd. 673 (2016) 441–454, doi:10.1016/J.JALLCOM.2016.02.251.
[19] G.B. Olson, M. Cohen, A general mechanism of martensitic nucleation: part II. FCC/BCC and other martensitic transformations, Metall. Trans. A 7 (11) (1976) 1905–1914, doi:10.1007/BF02654988.
[20] J.D. Eshelby, The elastic field outside an ellipsoidal inclusion, Proc. R. Soc. A: Math., Phys. Eng. Sci. 252 (1271) (1959) 561–569, doi:10.1098/rspa.1959.0173.
[21] E. Galindo-Nava, On the prediction of martensite formation in metals, Scr. Mater. 138 (2017) 6–11, doi:10.1016/J.SCRIPTAMAT.2017.05.026.
[22] J. Zhang, J. Li, Z. Chen, Q. Meng, F. Sun, B. Shen, Microstructural evolution of a ductile metastable β titanium alloy with combined TRIP/TWIP effects, J. Alloys Compd. 699 (2017) 775–782, doi:10.1016/J.JALLCOM.2016.12.394.
[23] G.B. Olson, M. Cohen, A general mechanism of martensitic nucleation: part II. FCC/BCC and other martensitic transformations, Metall. Trans. A 7 (11) (1976) 1905–1914, doi:10.1007/BF02654988.
[24] F. Kroupa, V. Vítek, Splitting of dislocations in b.c.c. metals on {110} planes, Czechoslov. J. Phys. 14 (5) (1964) 337–346, doi:10.1007/BF01689142.
[25] D. Hull, D.J. Bacon, Introduction to Dislocations, Butterworth-Heinemann, 2011.
[26] I. Weiss, S.L. Semiatin, Thermomechanical processing of beta titanium alloys - An overview, Mater. Sci. Eng. A 243 (1–2) (1998) 46–65, doi:10.1016/S0921-5093(97)00783-1.
[27] A. Dobromyslov, V. Elkin, Martensitic transformation and metastable β-phase in binary titanium alloys with d-metals of 4–6 periods, Scr. Mater. 44 (6) (2001) 905–910, doi:10.1016/S1359-6462(00)00694-1.
[28] P. Duwez, The martensite transformation temperature in titanium binary alloys., 1952. URL: http://www.dtic.mil/docs/citations/AD0493277
[29] K. Jepson, A. Brown, J. Gray, The effect of cooling rate on the beta transformation in Ti–Nb and Ti–Al alloys, in: The Science, Technology and Application of Titanium, Elsevier, 1970, pp. 677–690, doi:10.1016/B978-0-08-006564-9.50074-9.
[30] X. Ji, S. Emura, X. Min, K. Tsuchiya, Strain-rate effect on work-hardening behavior in β-type Ti–10Mo–1Fe alloy with TWIP effect, Mater. Sci. Eng.: A 707 (2017) 701–707, doi:10.1016/J.MSEA.2017.09.055.
[31] H. Liu, M. Niinomi, M. Nakai, J. Hieda, K. Cho, Changeable Young's modulus with large elongation-to-failure in β-type titanium alloys for spinal fixation applications, Scr. Mater. 82 (2014) 29–32, doi:10.1016/j.scriptamat.2014.03.014.
[32] M. Koul, J. Breedis, Phase transformations in beta isomorphous titanium alloys, Acta Metall. 18 (6) (1970) 579–588, doi:10.1016/0001-6160(70)90087-8.
[33] F. Sun, J. Zhang, M. Marteleur, T. Gloriant, P. Vermaut, D. Laillé, P. Castany, C. Curfs, P. Jacques, F. Prima, Investigation of early stage deformation mechanisms in a metastable β titanium alloy showing combined twinning-induced plasticity and transformation-induced plasticity effects, Acta Mater. 61 (17) (2013) 6406–6417, doi:10.1016/J.ACTAMAT.2013.07.019.
[34] S. Hanada, O. Izumi, Correlation of tensile properties, deformation modes, and phase stability in commercial β-phase titanium alloys, Metall. Trans. A 18 (2) (1987) 265–271, doi:10.1007/BF02825707.
[35] K. Endoh, M. Tahara, T. Inamura, H. Hosoda, Effect of Sn and Zr content on superelastic properties of Ti–Mo–Sn–Zr biomedical alloys, Mater. Sci. Eng.: A 704 (2017) 72–76, doi:10.1016/j.msea.2017.07.097.
[36] H.Y. Kim, S. Miyazaki, Martensitic transformation and superelastic properties of Ti–Nb base alloys, Mater. Trans. 56 (5) (2015) 625–634, doi:10.2320/matertrans.M2014454.
[37] S. Miyazaki, H.Y. Kim, P.J.S. Buenconsejo, Development of high temperature Ti–Ta shape memory alloys, in: ESOMAT 2009 - 8th European Symposium on Martensitic Transformations, EDP Sciences, Les Ulis, France, 2009, p. 01003, doi:10.1051/esomat/200901003.
[38] Z. Yang, X. Zheng, W. Cai, Martensitic transformation and shape memory effect of Ti–V–Al lightweight high-temperature shape memory alloys, Scr. Mater. 99 (2015) 97–100, doi:10.1016/J.SCRIPTAMAT.2014.11.038.
[39] Z. Yang, X. Zheng, Y. Wu, W. Cai, Martensitic transformation and shape memory behavior of Ti–V–Al–Fe lightweight shape memory alloys, J. Alloys Compd. 680 (2016) 462–466, doi:10.1016/J.JALLCOM.2016.04.151.
[40] E. Aeby-Gautier, A. Settefrati, F. Bruneseaux, B. Appolaire, B. Denand, M. Dehmas, G. Geandier, P. Boulet, Isothermal α formation in β metastable titanium alloys, J. Alloys Compd. 577 (2013) S439–S443, doi:10.1016/J.JALLCOM.2012.02.046.
[41] Y. Ohmori, T. Ogo, K. Nakai, S. Kobayashi, Effects of ω-phase precipitation on β–α, α transformations in a metastable β titanium alloy, Mater. Sci. Eng.: A 312 (1–2) (2001) 182–188, doi:10.1016/S0921-5093(00)01891-8.
[42] D.E. Laughlin, N.J. Jones, A.J. Schwartz, T.B. Massalski, Thermally activated martensite: its relationship to non-thermally activated (Athermal) martensite, in: ICOMAT, John Wiley & Sons, Inc., Hoboken, NJ, USA, 2013, pp. 141–144, doi:10.1002/9781118803592.ch19.
[43] A. Cottrell, An Introduction to Metallurgy, Edward Arnold, 1967.
[44] T. Grosdidier, C. Roubaud, M.-J. Philippe, Y. Combres, The deformation mechanisms in the β-metastable β-Cez titanium alloy, Scr. Mater. 36 (1) (1997) 21–28, doi:10.1016/S1359-6462(96)00341-7.
[45] Y. Yang, P. Castany, M. Cornen, F. Prima, S. Li, Y. Hao, T. Gloriant, Characterization of the martensitic transformation in the superelastic Ti–Nb–Zr–Sn alloy by in situ synchrotron X-ray diffraction and dynamic mechanical analysis, Acta Mater. 88 (2015) 25–33, doi:10.1016/j.actamat.2015.01.039.
[46] D.L. Moffat, D.C. Larbalestier, The competition between martensite and omega in quenched Ti–Nb alloys, Metall. Trans. A 19 (7) (1988) 1677–1686, doi:10.1007/BF02645135.
[47] S. Cai, J.E. Schaffer, Y. Ren, Deformation of a Ti–Nb alloy containing α"-martensite and omega phases, Appl. Phys. Lett. 106 (13) (2015) 131907, doi:10.1063/1.4916960.
[48] S. Neelakantan, P. Rivera-Díaz-del Castillo, S. van der Zwaag, Prediction of the martensite start temperature for β titanium alloys as a function of composition, Scr. Mater. 60 (8) (2009) 611–614, doi:10.1016/j.scriptamat.2008.12.034.
[49] G. Ghosh, G. Olson, Kinetics of F.C.C. B.C.C. heterogeneous martensitic nucleation. The critical driving force for athermal nucleation, Acta Metall. Mater. 42 (10) (1994) 3361–3370, doi:10.1016/0956-7151(94)90468-5.
[50] M. Umemoto, W.S. Owen, Effects of austenitizing temperature and austenite grain size on the formation of athermal martensite in an iron–nickel and an iron–nickel–carbon alloy, Metall. Trans. 5 (9) (1974) 2041–2046, doi:10.1007/BF02644497.
[51] S. van Bohemen, L. Morsdorf, Predicting the Ms temperature of steels with a thermodynamic based model including the effect of the prior austenite grain size, Acta Mater. 125 (2017) 401–415, doi:10.1016/J.ACTAMAT.2016.12.029.
[52] L. Lilensten, Y. Danard, C. Brozek, S. Mantri, P. Castany, T. Gloriant, P. Vermaut, F. Sun, R. Banerjee, F. Prima, On the heterogeneous nature of deformation in a strain-transformable beta metastable Ti–V–Cr–Al alloy, Acta Mater. 162 (2019) 268–276, doi:10.1016/J.ACTAMAT.2018.10.003.
[53] X. Min, S. Emura, T. Nishimura, K. Tsuchiya, K. Tsuzaki, Microstructure, tensile deformation mode and crevice corrosion resistance in Ti–10Mo–xFe alloys, Mater. Sci. Eng.: A 527 (21–22) (2010a) 5499–5506, doi:10.1016/J.MSEA.2010.06.016.
[54] X. Min, S. Emura, N. Sekido, T. Nishimura, K. Tsuchiya, K. Tsuzaki, Effects of Fe addition on tensile deformation mode and crevice corrosion resistance in Ti–15Mo alloy, Mater. Sci. Eng.: A 527 (10–11) (2010b) 2693–2701, doi:10.1016/J.MSEA.2009.12.050.

[55] M. Ahmed, D. Wexler, G. Casillas, D.G. Savvakin, E.V. Pereloma, Strain rate dependence of deformation-induced transformation and twinning in a metastable titanium alloy, Acta Mater. 104 (2016) 190–200, doi:10.1016/J.ACTAMAT.2015.11.026.

[56] T. Zhou, M. Aindow, S. Alpay, M. Blackburn, M. Wu, Pseudo-elastic deformation behavior in a Ti/Mo-based alloy, Scr. Mater. 50 (3) (2004) 343–348, doi:10.1016/J.SCRIPTAMAT.2003.10.012.

[57] L.C. Zhang, T. Zhou, M. Aindow, S.P. Alpay, M.J. Blackburn, M.H. Wu, Nucleation of stress-induced martensites in a Ti/Mo-based alloy, J. Mater. Sci. 40 (11) (2005) 2833–2836, doi:10.1007/s10853-005-2426-5.

[58] M. Niinomi, T. Hattori, K. Morikawa, T. Kasuga, A. Suzuki, H. Fukui, S. Niwa, Development of low rigidity β-type titanium alloy for biomedical applications, Mater. Trans. 43 (12) (2002) 2970–2977, doi:10.2320/matertrans.43.2970.

[59] C. Li, J. Chen, X. Wu, S. van der Zwaag, Effect of strain rate on stress-induced martensitic formation and the compressive properties of Ti–(Cr,Fe)–Al alloys, Mater. Sci. Eng.: A 573 (2013) 111–118, doi:10.1016/J.MSEA.2013.03.002.

[60] S. Sadeghpour, S. Abbasi, M. Morakabati, A. Kisko, L. Karjalainen, D. Porter, A new multi-element beta titanium alloy with a high yield strength exhibiting transformation and twinning induced plasticity effects, Scr. Mater. 145 (2018) 104–108, doi:10.1016/j.scriptamat.2017.10.017.

[61] F. Sun, Y. Hao, S. Nowak, T. Gloriant, P. Laheurte, F. Prima, A thermo-mechanical treatment to improve the superelastic performances of biomedical Ti–26Nb and Ti–20Nb–6Zr (at.%) alloys, J. Mech. Behav. Biomed. Mater. 4 (8) (2011) 1864–1872, doi:10.1016/J.JMBBM.2011.06.003.

[62] Y. Horiuchi, T. Inamura, H.Y. Kim, K. Wakashima, S. Miyazaki, H. Hosoda, Effect of boron concentration on martensitic transformation temperatures, stress for inducing martensite and slip stress of Ti-24 mol%Nb-3 mol%Al superelastic alloy, Mater. Trans. 48 (3) (2007) 407–413, doi:10.2320/matertrans.48.407.

[63] L. Chang, Y. Wang, Y. Ren, In-situ investigation of stress-induced martensitic transformation in Ti–Nb binary alloys with low Young's modulus, Mater. Sci. Eng.: A 651 (2016) 442–448, doi:10.1016/j.msea.2015.11.005.

[64] H.Y. Kim, J. Fu, H. Tobe, J.I. Kim, S. Miyazaki, Crystal structure, transformation strain, and superelastic property of Ti–Nb–Zr and Ti–Nb–Ta alloys, Shape Memory Superelast. 1 (2) (2015) 107–116, doi:10.1007/s40830-015-0022-3.

[65] R. Davis, H.M. Flower, D.R.F. West, Martensitic transformations in Ti–Mo alloys, J. Mater. Sci. 14 (3) (1979) 712–722, doi:10.1007/BF00772735.

[66] G.H. Narayanan, T.F. Archbold, Decomposition of the metastable beta phase in the all-beta alloy Ti–13V–11Cr–3Al, Metall. Trans. 1 (8) (1970) 2281–2290, doi:10.1007/BF02643446.

[67] A. Zafari, K. Xia, Stress induced martensitic transformation in metastable β Ti–5Al–5Mo–5V–3Cr alloy: triggering stress and interaction with deformation bands, Mater. Sci. Eng.: A 724 (2018) 75–79, doi:10.1016/J.MSEA.2018.03.070.

[68] G.M. Rusakov, A.V. Litvinov, V.S. Litvinov, Deformation twinning of titanium β-alloys of transition class, Metal Sci. Heat Treat. 48 (5–6) (2006) 244–251, doi:10.1007/s11041-006-0078-y.

[69] X. Wang, L. Li, W. Mei, W. Wang, J. Sun, Dependence of stress-induced omega transition and mechanical twinning on phase stability in metastable β Ti–V alloys, Mater. Charact. 107 (2015) 149–155, doi:10.1016/J.MATCHAR.2015.06.038.

[70] W. Wang, X. Zhang, J. Sun, Phase stability and tensile behavior of metastable β Ti–V–Fe and Ti–V–Fe–Al alloys, Mater. Charact. 142 (2018) 398–405, doi:10.1016/J.MATCHAR.2018.06.008.

[71] J. Lee Pak, C. Lei, C. Wayman, Atomic ordering in Ti–Al shape memory alloys, Mater. Sci. Eng.: A 132 (1991) 237–244, doi:10.1016/0921-5093(91)90380-6.

[72] E. Bertrand, P. Castany, T. Gloriant, Investigation of the martensitic transformation and the damping behavior of a superelastic Ti–Ta–Nb alloy, Acta Mater. 61 (2) (2013) 511–518, doi:10.1016/J.ACTAMAT.2012.09.065.

[73] E. Bertrand, Elaboration et caractérisation d'alliages biocompatibles Ti–Ta–Nb présentant des propriétés superélastiques et à mémoire de forme, http://www.theses.fr (2011). URL: https://www.theses.fr/2011ISAR0013

[74] S. Sadeghpour, S. Abbasi, M. Morakabati, Deformation-induced martensitic transformation in a new metastable β titanium alloy, J. Alloys Compd. 650 (2015) 22–29, doi:10.1016/j.jallcom.2015.07.263.

[75] F.-W. Ling, H.J. Rack, E.A. Starke, An X-ray examination of deformation in β Ti-V alloys, ESM Trans. 4 (7) (1973) 1671–1676.

[76] J. Zhang, J. Li, G. Chen, L. Liu, Z. Chen, Q. Meng, B. Shen, F. Sun, F. Prima, Fabrication and characterization of a novel β metastable Ti–Mo–Zr alloy with large ductility and improved yield strength, Mater. Charact. 139 (2018) 421–427, doi:10.1016/J.MATCHAR.2018.03.031.

[77] D.J. DeLazaro, M. Hansen, R.E. Riley, W. Rostoker, Time-temperature-transformation characteristics of titanium-molybdenum alloys, JOM 4 (3) (1952) 265–269, doi:10.1007/BF03397687.

[78] Y. Xu, D. Yi, H. Liu, X. Wu, B. Wang, F. Yang, Effects of cold deformation on microstructure, texture evolution and mechanical properties of Ti–Nb–Ta–Zr–Fe alloy for biomedical applications, Mater. Sci. Eng.: A 547 (2012) 64–71, doi:10.1016/J.MSEA.2012.03.081.

[79] D. Raabe, Omega phase acts as a switch between dislocation channeling and joint twinning-and transformation-induced plasticity in a metastable beta titanium alloy, URL: http://www.academia.edu/36333960/Omega_phase_acts_as_a_switch_between_dislocation_channeling_and_joint_twinning-and_transformation-induced_plasticity_in_a_metastable_beta_titanium_alloy

[80] L. Li, W. Mei, H. Xing, X. Wang, J. Sun, Zigzag configuration of mechanical twin and stress-induced omega phase in metastable β Ti–34Nb (at.%) alloy, J. Alloys Compd. 625 (2015) 188–192, doi:10.1016/j.jallcom.2014.11.082.

[81] Y.L. Zhou, M. Niinomi, T. Akahori, Effects of Ta content on Young–s modulus and tensile properties of binary Ti–Ta alloys for biomedical applications, Mater. Sci. Eng.: A 371 (1–2) (2004) 283–290, doi:10.1016/J.MSEA.2003.12.011.

[82] C. Brozek, F. Sun, P. Vermaut, Y. Millet, A. Lenain, D. Embury, P. Jacques, F. Prima, A β-titanium alloy with extra high strain-hardening rate: design and mechanical properties, Scr. Mater. 114 (2016) 60–64, doi:10.1016/J.SCRIPTAMAT.2015.11.020.

[83] H. Zhan, W. Zeng, G. Wang, D. Kent, M. Dargusch, On the deformation mechanisms and strain rate sensitivity of a metastable β Ti–Nb alloy, Scr. Mater. 107 (2015) 34–37, doi:10.1016/j.scriptamat.2015.05.014.

[84] L. Ren, W. Xiao, C. Ma, R. Zheng, L. Zhou, Development of a high strength and high ductility near β-Ti alloy with twinning induced plasticity effect, Scr. Mater. 156 (2018) 47–50, doi:10.1016/J.SCRIPTAMAT.2018.07.012.

[85] F. Zimmermann, M. Humbert, Determination of the habit plane characteristics in the β–α phase transformation induced by stress in Ti–Al–Sn–Zr-Mo–Cr–Fe, Acta Mater. 50 (7) (2002) 1735–1740, doi:10.1016/S1359-6454(02)00022-8.

[86] A. Biesiekierski, J. Lin, Y. Li, D. Ping, Y. Yamabe-Mitarai, C. Wen, Investigations into Ti–(Nb,Ta)–Fe alloys for biomedical applications, Acta Biomater. 32 (2016) 336–347, doi:10.1016/j.actbio.2015.12.010.

[87] E. Takahashi, T. Sakurai, S. Watanabe, N. Masahashi, S. Hanada, Effect of heat treatment and sn content on superelasticity in biocompatible tinbsn alloys, Mater. Trans. 43 (12) (2002) 2978–2983, doi:10.2320/matertrans.43.2978.

[88] S. Semboshi, T. Shirai, T.J. Konno, S. Hanada, In-situ transmission electron microscopy observation on the phase transformation of Ti–Nb–Sn shape memory alloys, Metall. Mater. Trans. A 39 (12) (2008) 2820–2829, doi:10.1007/s11661-008-9674-3.

[89] H. Kim, S. Hashimoto, J. Kim, H. H. M., 2004, Mechanical properties and shape memory behavior of Ti–Nb alloys, jstage.jst.go.jp, URL: https://www.jstage.jst.go.jp/article/matertrans/45/7/45_7_2443/_article/-char/ja/

[90] T. Shiraishi, K. Yubuta, T. Shishido., u. 2016, Elastic properties of as-solidified Ti–Zr binary alloys for biomedical applications, Mater. Trans., jstage.jst.go.jp, URL: https://www.jstage.jst.go.jp/article/matertrans/57/12/57_MI201501/_article/-char/ja/

[91] J.-Y. Yan, G. Olson, Molar volumes of bcc, hcp, and orthorhombic Ti-base solid solutions at room temperature, Calphad 52 (2016) 152–158, doi:10.1016/J.CALPHAD.2016.01.003.

[92] A. Dobromyslov, V. Elkin, The orthorhombic α–phase in binary titanium-base alloys with d-metals of V–VIII groups, Mater. Sci. Eng.: A 438–440 (2006) 324–326, doi:10.1016/J.MSEA.2006.02.086.

[93] B. Predel, Cr–Ti (Chromium-Titanium), in: Cr–Cs...Cu–Zr, Springer-Verlag, Berlin/Heidelberg, pp. 1–8. 10.1007/10086090_1022URL: http://materials.springer.com/lb/docs/sm_lbs_978-3-540-47417-3_1022